Available online at www.sciencedirect.com
SCIENCE DIRECT®
Journal of the Mechanics and Physics of Solids
54 (2006) 756–782
JOURNAL OF THE MECHANICS AND PHYSICS OF SOLIDS
www.elsevier.com/locate/jmps

The structural performance of the periodic truss

R.G. Hutchinson, N.A. Fleck*

Engineering Department, Cambridge University, Trumpington Street, Cambridge CB2 1PZ, UK

Received 28 June 2005; received in revised form 22 October 2005; accepted 26 October 2005

Abstract

Matrix methods of linear algebra are used to analyse the structural mechanics of the periodic pin-jointed truss by application of Bloch's theorem. Periodic collapse mechanisms and periodic states of self-stress are deduced from the four fundamental subspaces of the kinematic and equilibrium matrix for the periodic structure. The methodology developed is then applied to the Kagome lattice and the triangular–triangular (T–T) lattice. Both periodic collapse mechanisms and collapse mechanisms associated with uniform macroscopic straining are determined. It is found that the T–T lattice possesses only macroscopic strain-producing mechanisms, while the Kagome lattice possesses only periodic mechanisms which do not generate macroscopic strain. Consequently, the Kagome lattice can support all macroscopic stress states. The macroscopic stiffness of the Kagome and T–T trusses is obtained from energy considerations. The paper concludes with a classification of collapse mechanisms for periodic lattices.

Keywords: Structures; Porous material; Stability and bifurcation; Mechanisms; Self-stress

1. Introduction

Over the past decade, a range of commercial metallic foams have been developed, see for example, Ashby et al. (2000). These are mostly produced by the introduction of gas bubbles (e.g. hydrogen) into the melt. The bubble expansion process leads to random cellular structures, and minimisation of surface energy leads to a low nodal connectivity, with typically three to four cell struts per node as shown in Fig. 1a. It is generally

*Corresponding author. Tel.: +44 1223332650; fax: +44 1223765046.
E-mail address: naf1@cam.ac.uk (N.A. Fleck).

0022-5096/$ - see front matter © 2005 Elsevier Ltd. All rights reserved.
doi:10.1016/j.jmps.2005.10.008

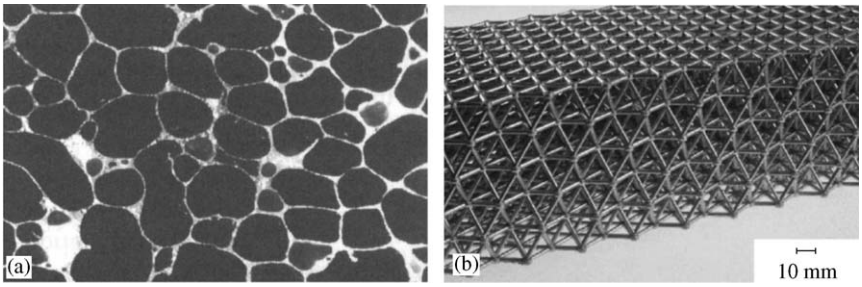

Fig. 1. (a) Planar section through an Alporas closed-cell metal foam of relative density $\rho/\rho_s = 0.09$ (from Ashby et al., 2000). (b) Photograph of the octet-truss lattice material made from a casting aluminium alloy, LM25 (from Deshpande et al., 2001b).

recognised that the resulting mechanical properties are far from optimal due to the fact that the cell walls deform by local bending (Ashby et al., 2000; Deshpande et al., 2001a). This has led to a search for open-cell microstructures which deform by the stretching of constituent cell members, giving a much higher stiffness and strength per unit mass. A photograph of the octet-truss structure is given in Fig. 1b. The joint positions of this Buckminster Fuller architecture (Marks, 1960) correspond to the face-centred cubic (FCC) crystal structure (Hilbert and Cohn-Vossen, 1990; Jones and March, 1973). The joint connectivity is 12, and this spatially periodic *lattice material* has the feature that the cell members deform by local stretching for all macroscopic loading states.[1] Consequently, the specific mechanical properties of the octet truss far exceed those of open-cell foams. The principal aim of this paper is to develop and apply systematic analytical procedures for the macroscopic properties of pin-jointed periodic lattice materials, such as the octet-truss structure.

The macroscopic effective properties of a rigid-jointed lattice are closely related to the structural performance of the pin-jointed parent structure. It is appreciated that practical lattice structures are neither pin-jointed nor rigid-jointed. Nonetheless, the pin-jointed truss can give useful physical insight as follows. Consider a slender bar, built-in at one end and subjected to a combined transverse and axial load at the other end. The built-in bar has a much lower transverse stiffness than axial stiffness. Consequently, the assumption of pin-joints remains a useful idealisation for the deformation response of lattice structures comprising slender bars. The pin-jointed version comprises bars which are stiff in stretching yet can rotate freely about the pin-joints. When the bar connectivity of the pin-joints is sufficiently low, the pin-jointed truss collapses by inextensional mechanisms; the rigid-jointed version deforms by bending of the bars and rotation of the joints. Alternatively, a high connectivity causes the pin-jointed truss to behave as a redundant structure and collapse now involves bar extension; a similar deformation mode is exhibited by the rigid-jointed version. We conclude that the structural performance of both the pin-jointed parent truss and the rigid-jointed daughter structure are largely dictated by the nodal connectivity. These concepts are made precise below for the periodic pin-jointed lattice.

[1]Here, and in the sequel, the macroscopic loading states considered are work conjugate to a state of uniform macroscopic strain, with rotation gradients ignored.

The structure of the paper is as follows. A structural analysis of pin-jointed lattices with extensible bars is developed, based upon the equilibrium matrix analysis methods of Pellegrino and Calladine (1986). Deformation of the periodic lattice is taken to be either periodic, in accordance with Bloch-wave theory, or is associated with uniform macroscopic straining (the Cauchy–Born hypothesis). Bloch-wave theory is used to identify both the periodic states of self-stress and the periodic collapse mechanisms which do not produce macroscopic strain. The assumption of uniform macroscopic straining is used to calculate the internal energy and the macroscopic stiffness of the lattice structure. The theory is then applied to the Kagome lattice and the triangular–triangular T–T lattice in order to obtain the collapse mechanisms, states of self-stress and the macroscopic effective stiffness.

2. Review of matrix analysis for pin-jointed trusses

A developed literature exists on the structural mechanics of *finite* pin-jointed trusses. Much less is known about the mechanics of *infinite*, periodic pin-jointed trusses. This is the subject of the present paper. Maxwell (1864) formulated the so-called Maxwell's rule for a finite pin-jointed truss: a 3D truss having j joints and no kinematic constraints requires at least $3j-6$ bars to have the possibility of rigidity. Pellegrino and Calladine (1986) generalised Maxwell's rule and showed how the methods of linear algebra may be applied to both planar and spatial trusses. More recently, Pellegrino (1993) formalised these methods within the framework of the singular value decomposition (SVD) and Deshpande et al. (2001a) examined the stiffness of various foam topologies. We base our review of matrix methods mainly upon Pellegrino and Calladine (1986) and Pellegrino (1993). First, we summarise the behaviour of finite pin-jointed structures and then we consider infinite, periodic structures.

2.1. Finite structures

We begin with some definitions. A finite truss of b bars and j pin-joints is *statically determinate* when the tension in every bar can be determined solely from the equilibrium equations for a given set of external forces applied to each joint; the number of equilibrium equations is equal to the number of unknown bar tensions. A finite truss is *kinematically determinate* when the location of each joint is uniquely determined by the length of each bar. If an unconstrained truss is statically and kinematically determinate then, by Maxwell (1864),

$$b-2j+3=0 \text{ in two-dimensions (2D)} \tag{1}$$

and

$$b-3j+6=0 \text{ in three-dimensions (3D).} \tag{2}$$

We emphasise that the relations (1) and (2) are *necessary*, but not *sufficient*, conditions for static and kinematic determinacy.

2.1.1. Equilibrium matrix

Before generalising (1) and (2), we first introduce the *equilibrium matrix* $\boldsymbol{A}$. Consider a planar truss (dimension $n=2$), or a spatial truss (dimension $n=3$) truss, consisting of j total joints connected by b bars and constrained by k *kinematic constraints* to rigid

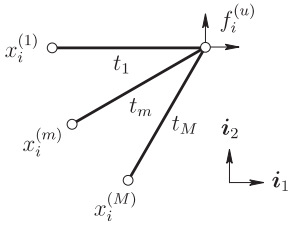

Fig. 2. Joint equilibrium in n-dimensions: t_m is the mth bar tension, $x_i^{(m)}$ is the ith position component of the mth joint and $f_i^{(u)}$ is the ith external force component applied at the joint u. All components are defined with respect to the usual orthonormal basis $\{\boldsymbol{i}_1,\ldots,\boldsymbol{i}_n\}$.

foundations. The b bar *tensions* are assembled into a vector $\boldsymbol{t}$, the $(nj-k)$ components of *external force* are assembled into a vector $\boldsymbol{f}$, the b bar *elongations* are assembled into a vector $\boldsymbol{e}$, and the $(nj-k)$ *displacement* components are assembled into a vector $\boldsymbol{d}$.

A representative, unconstrained joint u connected to M neighbouring joints by M bars is shown in Fig. 2. The equilibrium relations in n dimensions for this joint are

$$\sum_{m=1}^{M}\frac{(x_i^{(m)}-x_i^{(u)})\cdot t_m}{L_m}\equiv\sum_{m=1}^{M}C_i^{(m)}\cdot t_m=f_i^{(u)}\quad\forall i\in\{1,\ldots,n\}. \tag{3}$$

Here, t_m is the mth bar tension, $x_i^{(m)}$ is the ith position component of the mth joint, L_m is the length of the mth bar, $C_i^{(m)}$ is the ith component of the direction cosine vector of the mth bar, and $f_i^{(u)}$ is the ith external force component applied at the joint u. Now apply (3) to the j joints and b bars comprising a n-dimensional truss with k kinematic constraints. Then, the direction cosines, with u ranging over all j, are $C_i^{(m)}=(x_i^{(m)}-x_i^{(u)})/L_m$; they generate the real, $(nj-k)\times b$ equilibrium matrix $\boldsymbol{A}\in\mathbb{R}^{(nj-k)\times b}$. The bar tensions t_m range over all b and make up the real b-element tension vector $\boldsymbol{t}\in\mathbb{R}^b$; and, the right-hand side force components $f_i^{(u)}$ make up the $(nj-k)$ element load vector $\boldsymbol{f}\in\mathbb{R}^{nj-k}$. The equilibrium statements are written compactly in matrix form as

$$\boldsymbol{A}\cdot\boldsymbol{t}=\boldsymbol{f}. \tag{4}$$

2.1.2. Kinematic matrix

The kinematic equations conjugate to (3) and (4) are developed as follows. Introduce $\boldsymbol{d}\in\mathbb{R}^{nj-k}$ as the (infinitesimal) joint displacement vector and $\boldsymbol{e}\in\mathbb{R}^b$ as the bar elongation vector. Then,

$$e_m=\sum_{i=1}^{n}C_i^{(m)}\cdot(d_i^{(v)}-d_i^{(u)})\quad\forall m\in\{1,\ldots,b\}. \tag{5}$$

In matrix form, this reads

$$\boldsymbol{B}\cdot\boldsymbol{d}=\boldsymbol{e} \tag{6}$$

thereby defining the *kinematic matrix*, $\boldsymbol{B}\in\mathbb{R}^{b\times(nj-k)}$. Application of the principle of virtual work (PVW) implies that $\boldsymbol{B}=\boldsymbol{A}^{\mathrm{T}}$, where the superscript T denotes the transpose.

Pellegrino and Calladine (1986) have generalised Maxwell's rule by proving that the number of independent inextensional *mechanisms*, $m\geqslant 0$, and the number of independent

states of self-stress, $s \geqslant 0$, are related to the rank r of the equilibrium matrix $\boldsymbol{A}$ by

$$s = b - r \quad \text{and} \quad m = nj - k - r. \tag{7}$$

Note that s can be described qualitatively as the number of redundant bars in an arbitrary truss (see Crandall et al., 1978; Pellegrino and Calladine, 1986; Przemieniecki, 1968).

We now specialise (7) to the case of a free planar or spatial truss with $k = 0$. Then,

$$s = b - r \quad \text{and} \quad m = nj - r \tag{8}$$

and the null space of $\boldsymbol{A}$, $\text{Nul}(\boldsymbol{A}^{\text{T}})$, contains inextensional mechanisms that correspond to *rigid-body motions* of the *entire*, finite truss. In 2D and 3D there are, respectively, three and six independent translations and rotations of a rigid body. Thus, for $k = 0$, we define the number of rigid-body motions, m_r, as

$$m_r = \begin{cases} 3 & \text{when } n = 2, \\ 6 & \text{when } n = 3. \end{cases} \tag{9}$$

Write m_i as the number of *internal mechanisms*. Then, upon substituting (9) into (8) we have

$$m_i = m - m_r = nj - r - m_r. \tag{10}$$

A free truss with $k = 0$ is statically and kinematically determinate when $s = m_i = 0$.

2.2. Infinite periodic structures

Thus far we have considered finite truss structures where the number of constituent bars and joints are finite, and numerical calculation of the rank of the corresponding equilibrium matrix is straightforward. This approach is now extended to an infinite periodic truss.

Deshpande et al. (2001a) considered the case of a periodic truss in which all joints are *similarly situated*, such that the truss appears invariant when viewed from any joint. The corresponding Maxwell's rule is a function of the number of bars connected to each joint, termed the joint connectivity Z. Deshpande et al. (2001a) found a necessary, but not sufficient, condition for rigidity is $Z = 4$ in 2D and $Z = 6$ in 3D. In contrast, the necessary *and* sufficient conditions for the rigidity of 2D and 3D similarly situated trusses are $Z = 6$ and $Z = 12$ (Deshpande et al., 2001a). These connectivities correspond to the planar fully triangulated truss and spatial octet truss, respectively. Note that these rigid trusses contain redundant members, with $s \neq 0$ and $m_i = 0$. While the above theory provide useful rigidity criteria, the restriction to similarly situated periodic trusses is severe. In fact, the square truss and fully triangulated truss are the only similarly situated 2D lattices. In this paper, we shall consider periodic trusses which do not possess similarly situated joints.

Guest and Hutchinson (2003) have shown recently that a pin-jointed infinite lattice cannot be both statically and kinematically determinate. The pin-jointed analysis detailed below probes more general kinematics than those assumed by them but leads to the same conclusion. We invoke *Bloch's theorem* and form the set of all possible periodic mechanisms ranging over all possible wavelengths, as well as a restricted set of non-periodic mechanisms that produce macroscopic strains. Details on the background and applications of Bloch's theorem on a wide range of problems in theoretical physics are given in Bloch (1928), Lomont (1959), Cornwell (1997) and Cantrell (2000).

We shall also show, by the principle of virtual work, that our kinematic analysis gives rise to corresponding infinitesimal statics: we shall form the set of all possible periodic states of self-stress over all possible wavelengths, as well as non-periodic states of self-stress that produce macroscopic stresses.

The Bloch-wave extension to the matrix theory of pin-jointed trusses builds upon the work of Triantafyllidis and Schnaidt (1993) and Triantafyllidis and Schraad (1998) for two-dimensional periodic composites. Triantafyllidis and Schnaidt (1993) analysed the elastic stability of a rigid-jointed, square lattice. Using the beam-column form of the Euler–Bernoulli beam stiffness matrix (e.g. Coates et al., 1988; Livesley, 1975), they first considered the primitive unit cell as a *finite* structure of rigid-joints and elastic beams. To convert this finite problem to the desired problem of periodic, infinite extent, they assumed that the infinitesimal displacement and rotation fields of the rigid-joints are doubly periodic over the entire lattice. In contrast, in the current study, Bloch's theorem is applied to the kinematic and equilibrium matrices of the unit cell of a periodic, pin-jointed structure. The matrix methods of analysis developed by Pellegrino and Calladine (1986) for finite, pin-jointed structures are thereby extended to the periodic case, and periodic mechanisms and states of self-stress are obtained.

3. Bloch-wave mechanisms for periodic structures

The general theory is developed for a periodic 2D or 3D lattice, but for illustration, the theory is explained for the case of the 2D Kagome lattice shown in Fig. 3a. A representative unit cell of this lattice is given in Fig. 3b, with an alternative unit cell sketched in Fig. 3c. Consider a primitive unit cell of a periodic lattice, and define the *direct translational basis* $\{\boldsymbol{a}_k\}$ where $k \in \{1,\ldots,n\}$. Again, n is the dimension of the lattice, such that $n=2$ in 2D and $n=3$ in 3D. Translations of the unit cell by the basis vectors $\{\boldsymbol{a}_k\}$ tessellate the cell and allow it to fill space. Any neighbouring unit cell may be reached upon translating the reference unit cell by a *direct lattice translation vector* $\boldsymbol{x} \equiv x^k \boldsymbol{a}_k$, where x^k is any set of integer values. For the 2D unit cell of Fig. 3b, we sketch our choice of $\{\boldsymbol{a}_1, \boldsymbol{a}_2\}$ in Fig. 4a. Next, introduce the *joint basis* $\{\boldsymbol{j}_l\}$ $\forall l \in \{1,\ldots,J\}$ in order to define the location of the J independent joints of the unit cell. In the unit cell of Fig. 3b, there are three such joints ($J=3$) with joint vectors $\{\boldsymbol{j}_1,\boldsymbol{j}_2,\boldsymbol{j}_3\}$ as sketched in Fig. 4b. Joints of the unit cell are omitted from the joint basis when they coincide with joints obtained by translating the unit

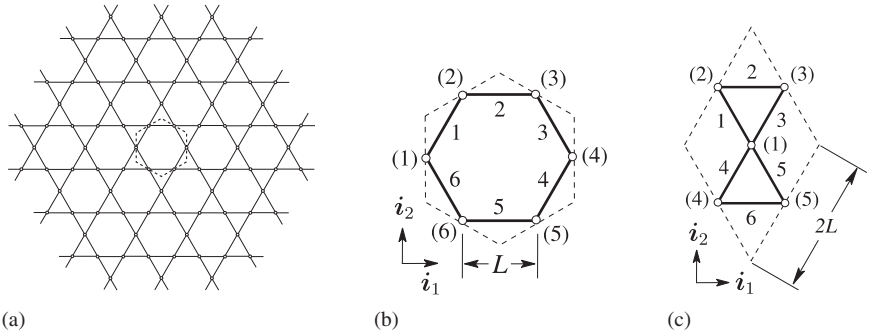

Fig. 3. (a) Kagome lattice with bar length L, (b) selected primitive unit cell and (c) alternate unit cell with labelling required for only joints 1, 2 and 3.

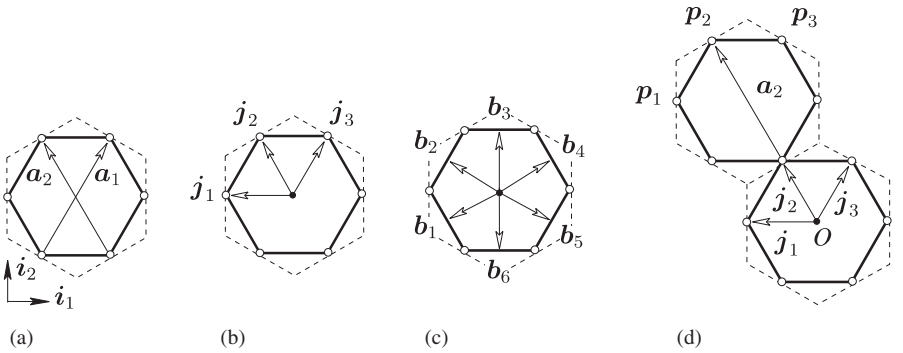

Fig. 4. Kagome lattice bases: (a) direct translation vectors, (b) joint vectors, (c) bar vectors, and (d) illustration of lattice position vectors. Each bar is of length L.

cell by some integer combination of $\{\boldsymbol{a}_k\}$. A bar basis $\{\boldsymbol{b}_m\}$ $\forall m \in \{1,\ldots,M\}$ is likewise introduced to define the location of the mid-point of the M independent bars of the unit cell, see Fig. 4c.

We use the direct lattice translation basis $\{\boldsymbol{a}_k\}$ $\forall k \in \{1,\ldots,n\}$ and the joint basis $\{\boldsymbol{j}_l\}$ $\forall l \in \{1,\ldots,J\}$ to define the *direct lattice position vectors* of *all* joints $\boldsymbol{p}_l$ $\forall l \in \{1,\ldots,J\}$. For example, consider joint 2 of the reference unit cell of Fig. 3b. Joints of type 2 in neighbouring unit cells are located by translating the reference unit cell an integer number of $\{\boldsymbol{a}_k\}$, as sketched in Fig. 4d. We label the set of all joint locations of type $l \in \{1,\ldots,J\}$ by $\boldsymbol{p}_l$. Thus,

$$\boldsymbol{p}_l = \boldsymbol{j}_l + \boldsymbol{x} = \boldsymbol{j}_l + x^k \boldsymbol{a}_k \quad \forall l \in \{1,\ldots,J\},\ \ k \in \{1,\ldots,n\}. \tag{11}$$

We shall also make use of the *reciprocal lattice* basis, $\{\boldsymbol{a}^k\}$ of spatial dimension n. It is related directly to the direct translational basis by $\boldsymbol{a}^j \cdot \boldsymbol{a}_k = \delta^j_k$ where δ^j_k is the usual Kronecker delta symbol (equal to unity when $j = k$, and zero otherwise).

3.1. Joint displacements

Periodic displacement fields of the pin-jointed lattice are now explored, and for simplicity we restrict our development to the two-dimensional case; the full 3D treatment follows immediately. We assume that the 2D joint displacement is complex, $\boldsymbol{d}(\boldsymbol{p}_l, \boldsymbol{w}) \in \mathbb{C}^2$, and is defined over the *entire* lattice using Bloch's theorem for the joint displacement field. First, introduce the wave vector $\boldsymbol{w} \equiv w_\alpha \boldsymbol{a}^\alpha$ with rational components $0 \leqslant w_\alpha < 1$, and $\alpha \in \{1,2\}$. Then, Bloch's theorem gives:

$$\boldsymbol{d}(\boldsymbol{p}_l, \boldsymbol{w}) \equiv \boldsymbol{d}(\boldsymbol{j}_l + \boldsymbol{x}, \boldsymbol{w}) = \boldsymbol{d}(\boldsymbol{j}_l, \boldsymbol{w}) \exp(2\pi \mathrm{i} \boldsymbol{w} \cdot \boldsymbol{x}) \quad \forall l \in \{1,\ldots,J\} \tag{12}$$

in terms of the complex number $\mathrm{i} \equiv \sqrt{-1}$. Note that the displacement field (12) is periodic and generates vanishing macroscopic strain; later we shall deal with the case of uniform macroscopic straining.

We now extend the matrix analysis of a finite pin-jointed truss to a periodic lattice of infinite extent. Consider a lattice primitive unit cell $\mathbb{Y}$ comprised of j pin-joints, within and on the unit cell boundary $\partial\mathbb{Y}$, and b truss members that intersect $\partial\mathbb{Y}$ only at their joint-ends. The Kagome lattice unit cell of Fig. 3b is such a unit cell. Upon making use of the

theory reviewed in Section 2, one may form the kinematic matrix $\boldsymbol{B} \in \mathbb{R}^{b\times 2j}$ assuming that the unit cell is free of external kinematic constraints ($k = 0$). Imposition of periodicity reduces the kinematic matrix relation as follows. Identify each of the p periodic joint pairs on $\partial\mathbb{Y}$ separated by unit-cell translation vectors,

$$\hat{\boldsymbol{x}} = \hat{x}^{\alpha}\boldsymbol{a}_{\alpha} \quad \forall \hat{x}^{\alpha} \in \{-1, 0, 1\}, \tag{13}$$

such that the number of *independent* joints is $J = j - p$. Thus, the linearly independent joint basis, $\{\boldsymbol{j}_l\}\ \forall l \in \{1, \ldots J\}$, defines the joint basis $\{\boldsymbol{j}_l + \hat{\boldsymbol{x}}_l\}$, of which p vectors are dependent. Applying these p dependencies to (12) yields p equations of the form

$$\boldsymbol{d}(\boldsymbol{j}_l + \hat{\boldsymbol{x}}_l, \boldsymbol{w}) = z(\boldsymbol{w}, \hat{\boldsymbol{x}}_l)\boldsymbol{d}(\boldsymbol{j}_l, \boldsymbol{w}), \tag{14}$$

where $z(\cdot,\cdot)$ is a scalar complex function defined as

$$z(\boldsymbol{w}, \hat{\boldsymbol{x}}_l) = \exp(2\pi \mathrm{i}\boldsymbol{w} \cdot \hat{\boldsymbol{x}}_l). \tag{15}$$

Now insert Eqs. (14) and (15) into the unit-cell kinematic matrix relation (6), wherein $\boldsymbol{B} \in \mathbb{R}^{b\times 2j}$, to obtain the *reduced* relation

$$\bar{\boldsymbol{B}}(\boldsymbol{w}) \cdot \bar{\boldsymbol{d}}(\boldsymbol{w}) = \bar{\boldsymbol{e}}(\boldsymbol{w}) \tag{16}$$

by elimination of $2p$ elements of $\boldsymbol{d}$. The vectors $\bar{\boldsymbol{d}}$ and $\bar{\boldsymbol{e}}$ contain a subset of the elements of $\boldsymbol{d}$ and $\boldsymbol{e}$, respectively. For general $\boldsymbol{w}$, we have $\bar{\boldsymbol{d}}(\boldsymbol{w}) \in \mathbb{C}^{2J}$, $\bar{\boldsymbol{B}}(\boldsymbol{w}) \in \mathbb{C}^{b\times 2J}$ and $\bar{\boldsymbol{e}}(\boldsymbol{w}) \in \mathbb{C}^{b}$.

The next step is the calculation of the four fundamental subspaces of $\bar{\boldsymbol{B}}(\boldsymbol{w})$: the interpretation of (16) closely parallels the interpretation of (6) as given by Pellegrino and Calladine (1986). The null space of $\bar{\boldsymbol{B}}(\boldsymbol{w})$, $\mathrm{Nul}(\bar{\boldsymbol{B}}(\boldsymbol{w}))$, is a linearly independent basis spanning all the joint displacement vectors $\bar{\boldsymbol{d}}$ compatible with zero bar elongations $\bar{\boldsymbol{e}} = \boldsymbol{0}$. Upon using (12), each such null vector $\bar{\boldsymbol{d}}$ defines a *periodic mechanism* of the lattice with wave vector $\boldsymbol{w}$. The row space of $\bar{\boldsymbol{B}}$, $\mathrm{Row}(\bar{\boldsymbol{B}}(\boldsymbol{w}))$, is a basis spanning all joint displacement vectors $\bar{\boldsymbol{d}}$ compatible with non-zero bar elongations $\bar{\boldsymbol{e}} \neq \boldsymbol{0}$. The column space of $\bar{\boldsymbol{B}}$, $\mathrm{Col}(\bar{\boldsymbol{B}}(\boldsymbol{w}))$, spans all geometrically compatible reduced bar elongation vectors $\bar{\boldsymbol{e}}$. The left null space of $\bar{\boldsymbol{B}}(\boldsymbol{w})$ is $\mathrm{Nul}(\bar{\boldsymbol{B}}^{\mathrm{H}}(\boldsymbol{w}))$ where the superscript H denotes the complex conjugate of the transpose. This left null space spans all geometrically incompatible bar elongation vectors $\bar{\boldsymbol{e}}$ for each assumed value of $\boldsymbol{w}$.

Finally, one may exploit the linearity of the above formulation and sum over all possible $\boldsymbol{w}$, and thereby obtain a Fourier series representation of joint displacements based upon (12):

$$\boldsymbol{d}(\boldsymbol{p}_l) = \boldsymbol{d}(\boldsymbol{j}_l + \boldsymbol{x}) = \sum_{\boldsymbol{w}\in\mathbb{W}} \boldsymbol{d}(\boldsymbol{j}_l, \boldsymbol{w}) \exp(2\pi \mathrm{i}\boldsymbol{w} \cdot \boldsymbol{x}) \quad \forall l \in \{1, \ldots, J\}. \tag{17}$$

In (17), the wave vector $\boldsymbol{w}$ can be restricted without loss of generality to the primitive unit cell $\mathbb{W}$ in reciprocal space, known as the first *Brillouin zone* (see Brillouin, 1946; Grosso and Pastori-Parravincini, 2000; Jones and March, 1973; Lomont, 1959).

3.2. Joint forces

A similar development applies to the statics of an infinite periodic truss. Begin by writing the equilibrium statement for the unit cell as $\boldsymbol{A} \cdot \boldsymbol{t} = \boldsymbol{f}$. Then, apply the periodic boundary conditions for joint forces $\boldsymbol{f}$ to obtain the reduced relation

$$\bar{\boldsymbol{A}}(\boldsymbol{w}) \cdot \bar{\boldsymbol{t}} = \bar{\boldsymbol{f}}. \tag{18}$$

The principle of virtual work implies $\bar{\boldsymbol{A}} = \bar{\boldsymbol{B}}^{\mathrm{H}}$. With this direct connection in place, the four fundamental subspaces of $\bar{\boldsymbol{A}}$ are related directly to the four fundamental subspaces of $\bar{\boldsymbol{B}}$. For example, the null space $\mathrm{Nul}(\bar{\boldsymbol{A}})$ is identical to $\mathrm{Nul}(\bar{\boldsymbol{B}}^{\mathrm{H}})$, the space of periodic states of self-stress.

4. Macroscopic strain-producing mechanisms

The Bloch-wave theory described in Section 3 gives the periodic joint displacement fields for an infinite periodic truss. However, macroscopic strain-producing mechanisms are also possible. Consider again the primitive unit cell $\mathbb{Y}$ of a periodic lattice, such as that given in Fig. 3b. The unit cell has j pin-joints within and on the unit cell boundary $\partial\mathbb{Y}$, and has b truss members that only contact $\partial\mathbb{Y}$ at their joint-ends. The *Cauchy–Born hypothesis* (Bhattacharya, 2003; Born and Huang, 1954; Maugin, 1992; Pitteri and Zanzotto, 2003) states that the infinitesimal displacement fields of the periodic truss can be additively decomposed into an affine deformation field of the joints as dictated by the macroscopically homogeneous strain $\bar{\boldsymbol{\varepsilon}}$, and into a displacement field which repeats from one cell to the next. Thus, the displacement field of any unit cell $\mathbb{Y}$ is

$$\boldsymbol{d}(\boldsymbol{j}_l + \hat{\boldsymbol{x}}_l) = \bar{\boldsymbol{\varepsilon}} \cdot \hat{\boldsymbol{x}}_l + \boldsymbol{p}(\boldsymbol{j}_l) \quad \forall \boldsymbol{j}_l \in \partial\mathbb{Y} \tag{19}$$

for all $l \in \{1, \ldots, J\}$ where the independent joint basis $\{\boldsymbol{j}_l\}$ was defined in Section 3 and the unit-cell translation basis $\{\hat{\boldsymbol{x}}_l\}$ has already been defined in (13). The vector field $\boldsymbol{p}(\boldsymbol{j}_l)$ is unit-cell periodic.

The periodicity statement (19) is applied to the unit cell kinematic matrix relation $\boldsymbol{B} \cdot \boldsymbol{d} = \boldsymbol{e}$ in order to give the reduced equation

$$\bar{\boldsymbol{B}} \cdot \bar{\boldsymbol{d}} = \bar{\boldsymbol{e}} \tag{20}$$

by elimination of $2p$ elements of $\boldsymbol{d}$. In general, $\bar{\boldsymbol{d}} \in \mathbb{C}^{2J}$, $\bar{\boldsymbol{B}} \in \mathbb{C}^{b \times 2J}$ and $\bar{\boldsymbol{e}} \in \mathbb{C}^{b}$. Note that $\bar{\boldsymbol{B}}$ is *identical* to the Bloch-wave reduced kinematic matrix of (16) for $\boldsymbol{w} = \boldsymbol{0}$; that is, $\bar{\boldsymbol{B}} = \bar{\boldsymbol{B}}(\boldsymbol{w} = \boldsymbol{0})$. The next step is again the calculation of the four fundamental subspaces of $\bar{\boldsymbol{B}}$. Details are given for specific lattices in the following sections.

The static boundary conditions consistent with the assumed kinematics (19) are that the *macroscopic tractions* $\bar{\boldsymbol{\sigma}} \cdot \boldsymbol{n}$ are equal and opposite on opposite faces of $\partial\mathbb{Y}$. Thus, $\bar{\boldsymbol{\sigma}} \cdot \boldsymbol{n}$ is *anti-periodic* over $\mathbb{Y}$. This may be expressed in terms of external joint forces on $\partial\mathbb{Y}$ as

$$\boldsymbol{f}(\boldsymbol{j}_l + \hat{\boldsymbol{x}}_l) + \boldsymbol{f}(\boldsymbol{j}_l) = \boldsymbol{0}. \tag{21}$$

Alternatively, the boundary conditions for the case where *bars*, rather than joints, are cut by the unit cell boundary become

$$t(\boldsymbol{b}_m + \hat{\boldsymbol{x}}_m) - t(\boldsymbol{b}_m) = 0, \tag{22}$$

where $t(\boldsymbol{b}_m)$ are bar tensions and $\{\boldsymbol{b}_m\}$ $\forall m \in \{1, \ldots, B\}$ is the independent bar basis of Section 3. A combination of (21) and (22) is enforced when *both* bars and joints exist on $\partial\mathbb{Y}$. Application of (21) and (22) to the unit cell equilibrium matrix relation $\boldsymbol{A} \cdot \boldsymbol{t} = \boldsymbol{f}$ gives the states of self-stress. Alternatively, these states are found in the null space of the Bloch-wave reduced equilibrium matrix at $\boldsymbol{w} = \boldsymbol{0}$.

5. Kagome lattice

The theoretical development of Sections 3 and 4 is now applied to the 2D Kagome lattice of bar length L, as sketched in Fig. 3. Hyun and Torquato (2002) have shown that the Kagome lattice has optimal in-plane stiffness amongst isotropic trusses with bars of equal side length. Indeed, in the "dilute limit" of low relative density, the Kagome lattice attains the Hashin–Shtrikman upper bound (Christensen, 2000; Hyun and Torquato, 2002; Torquato et al., 1998). Hutchinson and Fleck (2005) have recently explored the stiffness, strength and actuating properties of the Kagome truss, and have demonstrated its morphing capability. With the addition of suitable patch bars on the periphery, statically and kinematically determinate finite versions have been obtained, see for example, Symons et al. (2005).

Consider the periodic Kagome lattice, with unit cell as sketched in Fig. 3b. The direct and reciprocal bases can be expressed in terms of the orthonormal basis $\{\boldsymbol{i}_\alpha\}$ as

$$\boldsymbol{a}_1 = L\boldsymbol{i}_1 + L\sqrt{3}\boldsymbol{i}_2 \quad \text{and} \quad \boldsymbol{a}_2 = -L\boldsymbol{i}_1 + L\sqrt{3}\boldsymbol{i}_2, \tag{23}$$

$$\boldsymbol{a}^1 = (2L)^{-1}\boldsymbol{i}_1 + \left(2L\sqrt{3}\right)^{-1}\boldsymbol{i}_2 \quad \text{and} \quad \boldsymbol{a}^2 = (-2L)^{-1}\boldsymbol{i}_1 + \left(2L\sqrt{3}\right)^{-1}\boldsymbol{i}_2. \tag{24}$$

The joint basis for the Kagome lattice comprises the three vectors $\boldsymbol{j}_1 = (-\boldsymbol{i}_1 + 0\boldsymbol{i}_2)L$, $\boldsymbol{j}_2 = (-\boldsymbol{i}_1 + \sqrt{3}\boldsymbol{i}_2)L/2$, and $\boldsymbol{j}_3 = (\boldsymbol{i}_1 + \sqrt{3}\boldsymbol{i}_2)L/2$. Likewise, the bar basis is made up of the six vectors $\boldsymbol{b}_1 = (-3\boldsymbol{i}_1 - \sqrt{3}\boldsymbol{i}_2)L/4$, $\boldsymbol{b}_2 = (-3\boldsymbol{i}_1 + \sqrt{3}\boldsymbol{i}_2)L/4$, $\boldsymbol{b}_3 = (0\boldsymbol{i}_1 + \sqrt{3}\boldsymbol{i}_2)L/2$, $\boldsymbol{b}_4 = (3\boldsymbol{i}_1 + \sqrt{3}\boldsymbol{i}_2)L/4$, $\boldsymbol{b}_5 = (3\boldsymbol{i}_1 - \sqrt{3}\boldsymbol{i}_2)L/4$ and $\boldsymbol{b}_6 = (0\boldsymbol{i}_1 + \sqrt{3}\boldsymbol{i}_2)L/2$.

We next form the kinematic relation $\boldsymbol{B}\cdot\boldsymbol{d} = \boldsymbol{e}$ for the Kagome lattice unit cell of Fig. 3b using the prescription (6). The components of this relation, for the choice of orthonormal basis $\{\boldsymbol{i}_1, \boldsymbol{i}_2\}$, read

$$\boldsymbol{B} = \begin{pmatrix} -\frac{1}{2} & -\frac{\sqrt{3}}{2} & \frac{1}{2} & \frac{\sqrt{3}}{2} & 0 & 0 & 0 & 0 & 0 & 0 & 0 & 0 \\ 0 & 0 & -1 & 0 & 1 & 0 & 0 & 0 & 0 & 0 & 0 & 0 \\ 0 & 0 & 0 & 0 & -\frac{1}{2} & \frac{\sqrt{3}}{2} & \frac{1}{2} & -\frac{\sqrt{3}}{2} & 0 & 0 & 0 & 0 \\ 0 & 0 & 0 & 0 & 0 & 0 & \frac{1}{2} & \frac{\sqrt{3}}{2} & -\frac{1}{2} & -\frac{\sqrt{3}}{2} & 0 & 0 \\ 0 & 0 & 0 & 0 & 0 & 0 & 0 & 0 & 1 & 0 & -1 & 0 \\ -\frac{1}{2} & \frac{\sqrt{3}}{2} & 0 & 0 & 0 & 0 & 0 & 0 & 0 & 0 & \frac{1}{2} & -\frac{\sqrt{3}}{2} \end{pmatrix}, \tag{25}$$

$$\boldsymbol{d}^{\mathrm{T}} = [d_1^{(1)}\ d_2^{(1)}\ d_1^{(2)}\ d_2^{(2)}\ d_1^{(3)}\ d_2^{(3)}\ d_1^{(4)}\ d_2^{(4)}\ d_1^{(5)}\ d_2^{(5)}\ d_1^{(6)}\ d_2^{(6)}], \tag{26}$$

and

$$\boldsymbol{e}^{\mathrm{T}} = [e_1\ e_2\ e_3\ e_4\ e_5\ e_6]. \tag{27}$$

The bar elongations are $e_k = e(\boldsymbol{b}_k)$ for $k \in \{1, 2, \ldots, 6\}$, $d_\alpha^{(l)} = d_\alpha(\boldsymbol{j}_l)$ for $l \in \{1, 2, 3\}$, $d_\alpha^{(4)} = d_\alpha(\boldsymbol{j}_1 + \boldsymbol{a}_1 - \boldsymbol{a}_2)$, $d_\alpha^{(5)} = d_\alpha(\boldsymbol{j}_2 - \boldsymbol{a}_2)$, and $d_\alpha^{(6)} = d_\alpha(\boldsymbol{j}_3 - \boldsymbol{a}_1)$.

The corresponding finite equilibrium matrix $\boldsymbol{A}$ is $\boldsymbol{A} = \boldsymbol{B}^{\mathrm{T}}$, such that $\boldsymbol{A}\cdot\boldsymbol{t} = \boldsymbol{f}$ for the unit cell of Fig. 3b. Here, $t_k = t(\boldsymbol{b}_k)$ for $k \in \{1, 2, \ldots, 6\}$, $f_\alpha^{(l)} = f_\alpha(\boldsymbol{j}_l)$ for $l \in \{1, 2, 3\}$, $f_\alpha^{(4)} = f_\alpha(\boldsymbol{j}_1 + \boldsymbol{a}_1 - \boldsymbol{a}_2)$, $f_\alpha^{(5)} = f_\alpha(\boldsymbol{j}_2 - \boldsymbol{a}_2)$, and $f_\alpha^{(6)} = f_\alpha(\boldsymbol{j}_3 - \boldsymbol{a}_1)$. The joint force vector components are defined using the orthonormal basis $\{\boldsymbol{i}_1, \boldsymbol{i}_2\}$ shown in Fig. 3b, giving $\boldsymbol{f}(\boldsymbol{j}_1) = f_\alpha(\boldsymbol{j}_1)\boldsymbol{i}_\alpha$ for example.

5.1. Bloch-wave reduction of the kinematic matrix

We proceed by using Bloch's theorem (12) to represent the joint displacements of the Kagome lattice as

$$\boldsymbol{d}(\boldsymbol{p}_l, \boldsymbol{w}) = \boldsymbol{d}(\boldsymbol{j}_l + \boldsymbol{x}, \boldsymbol{w}) = \boldsymbol{d}(\boldsymbol{j}_l, \boldsymbol{w}) \exp(2\pi \mathrm{i} \boldsymbol{w} \cdot \boldsymbol{x}) \quad \forall l \in \{1, 2, 3\}. \tag{28}$$

With a view towards the Bloch wave reduction of $\boldsymbol{B}$, periodicity demands

$$d_\alpha^{(4)} = z_1(\boldsymbol{w}) z_2^*(\boldsymbol{w}) d_\alpha^{(1)}, \quad d_\alpha^{(5)} = z_2^*(\boldsymbol{w}) d_\alpha^{(2)} \quad \text{and} \quad d_\alpha^{(6)} = z_1^*(\boldsymbol{w}) d_\alpha^{(3)}, \tag{29}$$

where $z_\alpha(\boldsymbol{w}) = \exp(2\pi \mathrm{i} w_\alpha)$ and $\alpha \in \{1, 2\}$. Here and in the following a superscript asterisk denotes the complex conjugate. Upon substituting (29) into $\boldsymbol{B} \cdot \boldsymbol{d} = \boldsymbol{e}$ as given by (25)–(27), the Bloch-wave reduced kinematic statement for the Kagome lattice, $\bar{\boldsymbol{B}}(\boldsymbol{w}) \cdot \bar{\boldsymbol{d}}(\boldsymbol{w}) = \bar{\boldsymbol{e}}(\boldsymbol{w})$, is explicitly

$$\begin{pmatrix} -\frac{1}{2} & -\frac{\sqrt{3}}{2} & \frac{1}{2} & \frac{\sqrt{3}}{2} & 0 & 0 \\ 0 & 0 & -1 & 0 & 1 & 0 \\ \frac{1}{2} z_1 z_2^* & -\frac{\sqrt{3}}{2} z_1 z_2^* & 0 & 0 & -\frac{1}{2} & \frac{\sqrt{3}}{2} \\ \frac{1}{2} z_1 z_2^* & \frac{\sqrt{3}}{2} z_1 z_2^* & -\frac{1}{2} z_2^* & -\frac{\sqrt{3}}{2} z_2^* & 0 & 0 \\ 0 & 0 & z_2^* & 0 & -z_1^* & 0 \\ -\frac{1}{2} & \frac{\sqrt{3}}{2} & 0 & 0 & \frac{1}{2} z_1^* & -\frac{\sqrt{3}}{2} z_1^* \end{pmatrix} \begin{Bmatrix} d_1^{(1)} \\ d_2^{(1)} \\ d_1^{(2)} \\ d_2^{(2)} \\ d_1^{(3)} \\ d_2^{(3)} \end{Bmatrix} = \begin{Bmatrix} e_1 \\ e_2 \\ e_3 \\ e_4 \\ e_5 \\ e_6 \end{Bmatrix}. \tag{30}$$

It is emphasised that the complex numbers $z_\alpha = \exp(2\pi \mathrm{i} w_\alpha)$ are directly related to the components w_α of the wave vector $\boldsymbol{w}$. It remains to search for those values of w_α for which periodic collapse mechanisms exist. Upon noting that the reduced kinematic matrix $\bar{\boldsymbol{B}}(\boldsymbol{w})$ in (30) is square, we conclude that periodic collapse mechanisms exist when $\bar{\boldsymbol{B}}(\boldsymbol{w})$ is singular. The number of independent periodic collapse mechanisms is given by the dimension of the null space of $\bar{\boldsymbol{B}}(\boldsymbol{w})$. Elementary row operations on $\bar{\boldsymbol{B}}$ yield the following augmented kinematic matrix:

$$\left(\begin{array}{cccccc|c} -\frac{1}{2} & -\frac{\sqrt{3}}{2} & \frac{1}{2} & \frac{\sqrt{3}}{2} & 0 & 0 & e_1 \\ 0 & \sqrt{3} & -\frac{1}{2} & -\frac{\sqrt{3}}{2} & \frac{1}{2} z_1^* & -\frac{\sqrt{3}}{2} z_1^* & -e_1 + e_6 \\ 0 & 0 & -1 & 0 & 1 & 0 & e_2 \\ 0 & 0 & \frac{1}{2}(z_1 - 1) & \frac{\sqrt{3}}{2}(z_1 - 1) & 0 & 0 & z_1 e_1 + z_2 e_4 \\ 0 & 0 & 0 & 0 & \frac{1}{2}(z_2^* - 1) & -\frac{\sqrt{3}}{2}(z_2^* - 1) & e_3 + z_1 z_2^* e_6 \\ 0 & 0 & 0 & 0 & z_2^* - z_1^* & 0 & z_2^* e_2 + e_5 \end{array}\right). \tag{31}$$

Examination of (31) reveals that $\bar{\boldsymbol{B}}(\boldsymbol{w})$ is singular when the determinant of the lower right-hand corner 4×4 matrix within the 6×6 kinematic matrix (31) is zero. Recalling the definition $\boldsymbol{w} = w_\alpha \boldsymbol{a}^\alpha$ and the periodicity relations (29), $\bar{\boldsymbol{B}}(\boldsymbol{w})$ is singular for the following choices of z_α: (i) $z_1(\boldsymbol{w}) = z_2(\boldsymbol{w})$, (ii) $z_1(\boldsymbol{w}) = 1$, or (iii) $z_2(\boldsymbol{w}) = 1$. In wave vector space, these three conditions become (i) $w_1 = w_2$, (ii) $w_1 = 0$, or (iii) $w_2 = 0$.

The collapse mechanisms for each of these trajectories in (w_1, w_2) space are now detailed. Without loss of generality, we exploit the symmetry of the Kagome lattice in order to present our findings. The first Brillouin zone (BZ) of the Kagome lattice, with its hexagonal ($\mathbb{D}_6$) symmetry, is sketched Fig. 5a. Symmetry dictates that one-twelfth of the

zone is fully representative: this sector is shown shaded in Fig. 5a and is given in more detail in Fig. 5b, with the locus (i) $w_1 = w_2$ included. Note that the loci (ii) $w_1 = 0$ and (iii) $w_2 = 0$ are obtained immediately from the solution for locus (i) via a rotation of $\pi/3$ and $-\pi/3$ radians, respectively. The collapse mechanisms (and corresponding states of self-stress, to be introduced below) along all three loci are summarised in Table 1 for completeness.

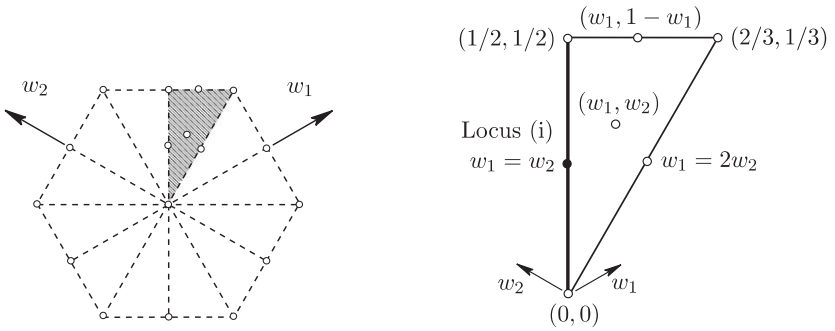

Fig. 5. Kagome lattice: (a) first Brillouin zone (BZ) with (b) one-twelfth shaded section and wave vector locus (i) $w_1 = w_2$ labelled.

Table 1
Kagome lattice: null vectors of the Bloch-wave reduced equilibrium ($\bar{\boldsymbol{A}}$) and kinematic ($\bar{\boldsymbol{B}}$) matrices

(w_1, w_2)	$\bar{\boldsymbol{d}} \in \mathrm{Nul}(\bar{\boldsymbol{B}})$ and $\bar{\boldsymbol{t}} \in \mathrm{Nul}(\bar{\boldsymbol{A}})$
$(0,0)$	$d_1^{(1)} = d_1^{(2)} = d_1^{(3)}; d_2^{(1)} = d_2^{(2)} = d_2^{(3)} = 0$ $t_1 = t_4; t_2 = t_3 = t_5 = t_6 = 0$
$(0,0)$	$d_2^{(1)} = d_2^{(2)} = d_2^{(3)}; d_1^{(1)} = d_1^{(2)} = d_1^{(3)} = 0$ $t_2 = t_5; t_1 = t_3 = t_4 = t_6 = 0$
$(0,0)$	$\frac{1}{2}d_1^{(1)} = -d_1^{(2)} = \frac{1}{\sqrt{3}}d_2^{(2)} = -d_1^{(3)} = -d_2^{(3)}; d_2^{(1)} = 0$ $t_3 = t_6; t_1 = t_2 = t_4 = t_5 = 0$
Locus (i) $0 < w_1 = w_2 \leqslant \frac{1}{2}$	$\sqrt{3}d_2^{(3)} = -\sqrt{3}d_2^{(2)} = d_1^{(3)} = d_1^{(2)}; d_1^{(1)} = d_2^{(1)} = 0$ $t_2 = t_5 \exp(2\pi \mathrm{i} w_1); t_1 = t_3 = t_4 = t_6 = 0$
Locus (ii) $w_1 = 0 < w_2 \leqslant \frac{1}{2}$	$\frac{1}{2}d_2^{(2)} = d_2^{(1)} = \frac{1}{\sqrt{3}}d_1^{(1)}; d_1^{(2)} = d_1^{(3)} = d_2^{(3)} = 0$ $t_1 = t_4 \exp(2\pi \mathrm{i} w_2); t_2 = t_3 = t_5 = t_6 = 0$
Locus (iii) $w_2 = 0 < w_1 \leqslant \frac{1}{2}$	$d_2^{(1)} = -\frac{1}{\sqrt{3}}d_1^{(1)} = d_2^{(3)} \exp(-2\pi \mathrm{i} w_1); d_1^{(2)} = d_2^{(2)} = d_1^{(3)} = 0$ $t_3 = t_6 \exp(2\pi \mathrm{i} w_1); t_1 = t_2 = t_4 = t_5 = 0$
Other (w_1, w_2)	$\bar{\boldsymbol{d}} = \emptyset$ $\bar{\boldsymbol{t}} = \emptyset$

5.2. Representative collapse mechanisms

The collapse mechanisms along the locus (i) satisfy $w_1 = w_2$ with $0 < w_1 \leqslant \frac{1}{2}$. At any general joint on the locus, a single collapse mechanism can operate, and the relative magnitude of each component of $\bar{\boldsymbol{d}}$ is stated in Table 1. Recall that the Bloch-wave analysis assumes complex displacements, and each value of joint displacement can be scaled arbitrarily by $d_1^{(2)}$, say. Here we set $d_1^{(2)}$ to equal unity and generate all other displacements by the connection given in Table 1 and in (28). Without loss of generality, two mechanisms emerge: one represented by the real components of the displacements, and one by the imaginary components. An example is shown in Fig. 6 for the choice $w_1 = w_2 = \frac{1}{3}$. To aid visualisation, an *equivalent* mechanism is sketched for each collapse mechanism. The equivalent mechanism comprises an assembly of rotating and translating discs which roll over each other. Their diameter can vary from one layer to the next, including the extreme case of stationary strips, see Fig. 6b. Next, consider the extremes of the locus (i), as set by $w_1 = w_2 = 0$ and $w_1 = w_2 = \frac{1}{2}$. The exponential modulation factor in (28) is then real. At $w_1 = w_2 = 0$, *three* mechanisms exist. Two are rigid-body modes but the third is a unit-cell

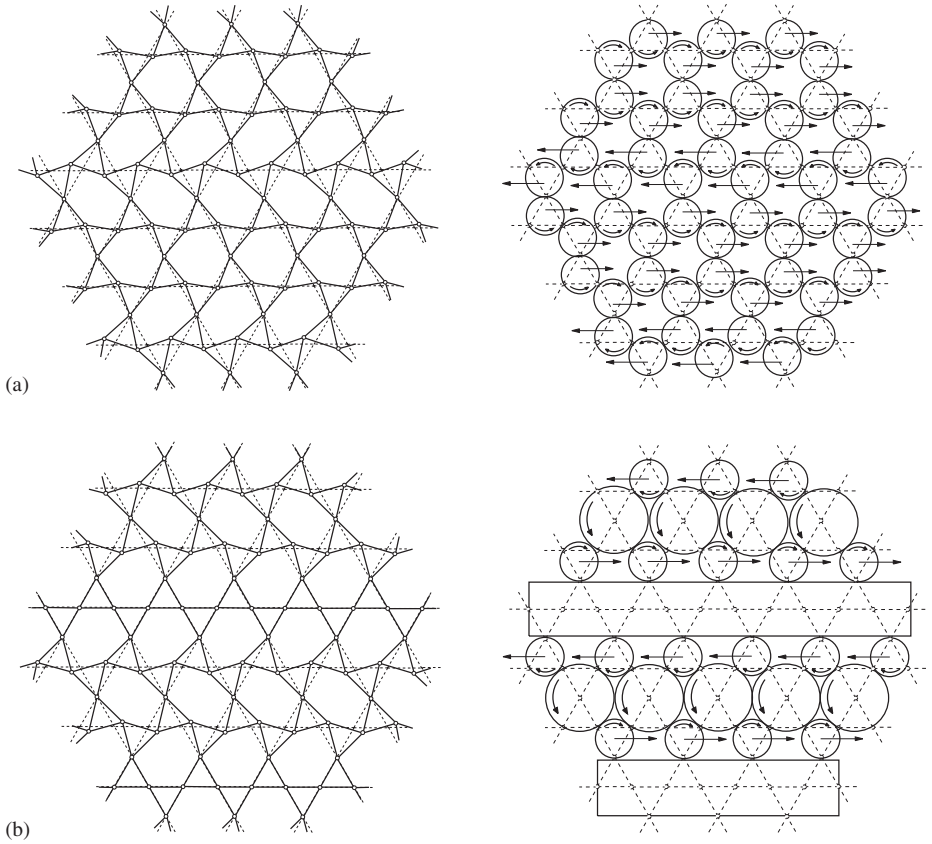

Fig. 6. Kagome lattice infinitesimal mechanisms (left) with an equivalent mechanism of rotating, rigid disks (right). Two mechanisms exist for $w_1 = w_2 = \frac{1}{3}$.

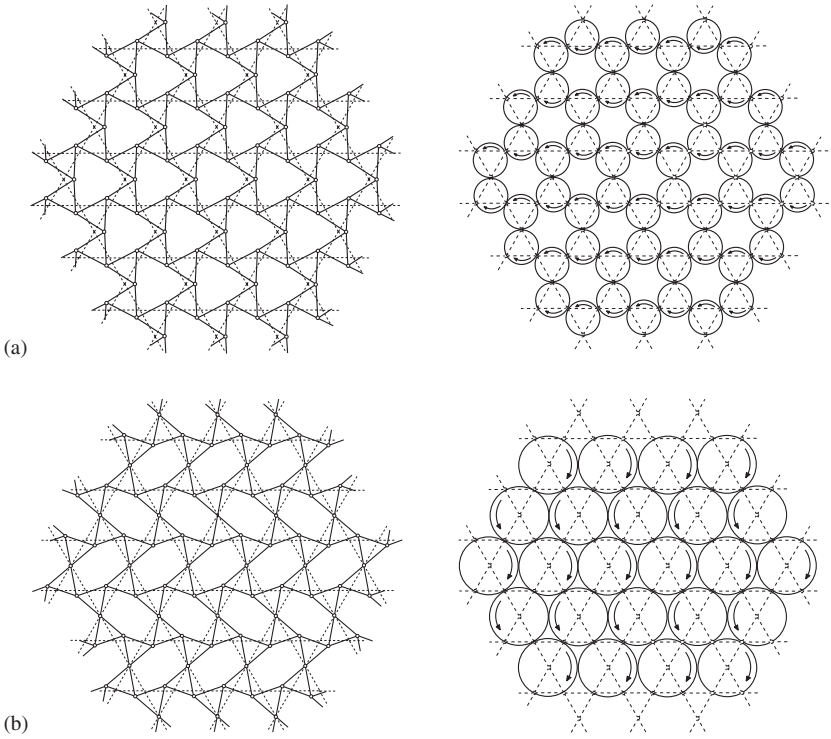

Fig. 7. Kagome lattice infinitesimal mechanisms (left) with equivalent mechanisms of rotating, rigid disks (right). (a) Mechanism for $w_1 = w_2 = 0$ and (b) mechanism for $w_1 = w_2 = \frac{1}{2}$.

periodic collapse mode. It is sketched in Fig. 7a, along with its equivalent mechanism. We shall show below that this mechanism is identical to the collapse mechanism associated with the Cauchy–Born hypothesis at zero macroscopic strain ($\bar{\boldsymbol{\varepsilon}} = \mathbf{0}$). Further, this mechanism has the property that it is the first increment of a *finite* collapse mechanism. A single collapse mode is also obtained at $w_1 = w_2 = \frac{1}{2}$. This has a wavelength of two unit cells and is sketched in Fig. 7b along with its equivalent mechanism.

It is instructive to compare the predictions in the present study with the combined experimental and numerical study by Tantikom et al. (2004). They examined the elastic–plastic transverse compression of a hexagonal array of bonded copper tubes, and they report the collapse mechanisms. The asymmetric deformation mode given in Fig. 11 of their paper is essentially the same collapse mechanism as that shown in Fig. 7b of the present study.

5.3. Bloch-wave reduction of the equilibrium matrix

A similar Bloch-wave reduction can be performed on the equilibrium matrix $\boldsymbol{A} = \boldsymbol{B}^{\mathrm{T}}$ for the periodic Kagome lattice. The reduction gives $\bar{\boldsymbol{A}}(\boldsymbol{w}) \cdot \bar{\boldsymbol{t}}(\boldsymbol{w}) = \bar{\boldsymbol{f}}(\boldsymbol{w})$, with $\bar{\boldsymbol{A}} \in \mathbb{C}^{6\times 6}$, $\bar{\boldsymbol{t}} \in \mathbb{C}^{6}$

and $\bar{\boldsymbol{f}} \in \mathbb{C}^6$ given by

$$\bar{\boldsymbol{A}}(\boldsymbol{w}) = \begin{pmatrix} -\frac{1}{2} & 0 & \frac{1}{2}z_1^* z_2 & \frac{1}{2}z_1^* z_2 & 0 & -\frac{1}{2} \\ -\frac{\sqrt{3}}{2} & 0 & -\frac{\sqrt{3}}{2}z_1^* z_2 & \frac{\sqrt{3}}{2}z_1^* z_2 & 0 & \frac{\sqrt{3}}{2} \\ \frac{1}{2} & -1 & 0 & -\frac{1}{2}z_2 & z_2 & 0 \\ \frac{\sqrt{3}}{2} & 0 & 0 & -\frac{\sqrt{3}}{2}z_2 & 0 & 0 \\ 0 & 1 & -\frac{1}{2} & 0 & -z_1 & \frac{1}{2}z_1 \\ 0 & 0 & \frac{\sqrt{3}}{2} & 0 & 0 & -\frac{\sqrt{3}}{2}z_1 \end{pmatrix}, \tag{32}$$

$$\bar{\boldsymbol{t}}^{\mathrm{T}} = [t_1 \;\; t_2 \;\; t_3 \;\; t_4 \;\; t_5 \;\; t_6] \tag{33}$$

and

$$\bar{\boldsymbol{f}} = \begin{Bmatrix} \boldsymbol{f}^{(1)} + z_1^* z_2 \boldsymbol{f}^{(4)} \\ \boldsymbol{f}^{(2)} + z_2 \boldsymbol{f}^{(5)} \\ \boldsymbol{f}_1^{(3)} + z_1 \boldsymbol{f}_1^{(6)} \end{Bmatrix}. \tag{34}$$

The principle of virtual work may be invoked to show directly that $\bar{\boldsymbol{A}}(\boldsymbol{w}) \equiv \bar{\boldsymbol{B}}^{\mathrm{H}}(\boldsymbol{w})$. Periodic states of self-stress given by the null space of $\bar{\boldsymbol{A}}$ are included in Table 1. Again, they exist along the wave vector loci (i) $w_1 = w_2$, (ii) $w_1 = 0$, or (iii) $w_2 = 0$.

As noted above we need consider loci (ii) and (iii) no further, as locus (i) is canonical. Along locus (i), a state of self-stress exists for any given value of $w_1 = w_2$ over the domain $0 < w_1 < \frac{1}{2}$. As for the collapse mechanisms, the state of self-stress is complex, and can be interpreted as two independent states, one given by the real part and the other given by the imaginary part of the solution. Without loss of generality, we set t_5 to equal unity in the prescription recorded in Table 1. The two states of self-stress at a representative point $w_1 = w_2 = \frac{1}{3}$ are shown in Fig. 8. The behaviour differs from the general case at the extremes of locus (i). At $w_1 = w_2 = 0$, three states of self-stress exist. They are sketched in Fig. 9a–c, and we shall show below that they are identical to the three states of self-stress

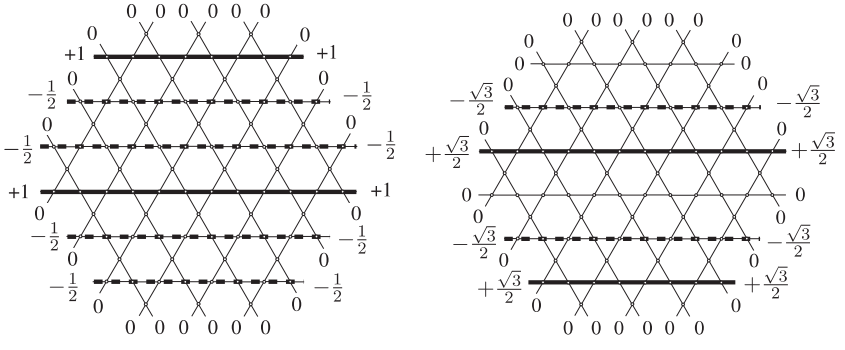

Fig. 8. Two states of self-stress in the Kagome lattice for $w_1 = w_2 = \frac{1}{3}$.

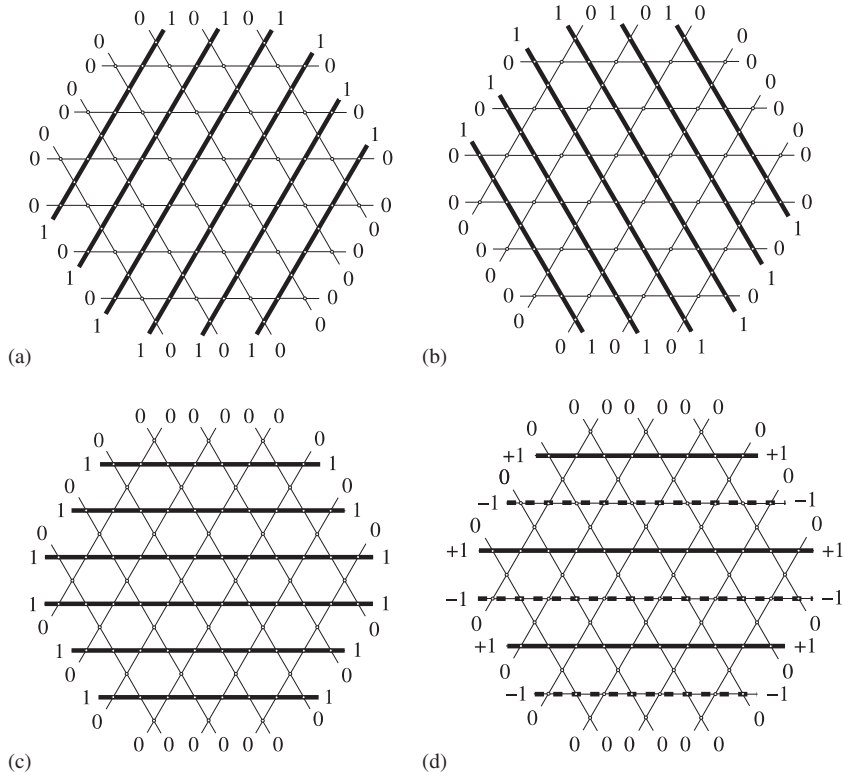

Fig. 9. (a–c) Three states of self-stress in the Kagome lattice for $w_1 = w_2 = 0$; (d) state of self-stress for $w_1 = w_2 = \frac{1}{2}$.

under the Cauchy–Born hypothesis. At the other limit of $w_1 = w_2 = \frac{1}{2}$, a single state of self-stress exists, see Fig. 9d.

5.4. Mechanisms which generate macroscopic strain

5.4.1. Cauchy–Born reduction of the kinematic matrix

Strain-producing collapse mechanisms are identified by applying the Cauchy–Born hypothesis (19) to the kinematics of the Kagome truss. Write the displacement of the six joints of the primitive unit cell as $d_\alpha^{(l)}$ for $l \in \{1,\ldots,6\}$ on the basis $\{\boldsymbol{i}_1, \boldsymbol{i}_2\}$, and let $\bar{\boldsymbol{\varepsilon}}$ denote the imposed macroscopic strain, with $\boldsymbol{p}(\boldsymbol{j}_l)$ periodic over the unit cell. We specialise (19) to the primitive Kagome lattice unit cell of Fig. 3b and find that for all $\alpha \in \{1,2\}$,

$$\left.\begin{aligned} d_\alpha^{(4)} - d_\alpha^{(1)} &= 2L\bar{\varepsilon}_{\alpha 1} \\ d_\alpha^{(5)} - d_\alpha^{(2)} &= L\bar{\varepsilon}_{\alpha 1} - L\sqrt{3}\bar{\varepsilon}_{\alpha 2} \\ d_\alpha^{(6)} - d_\alpha^{(3)} &= -L\bar{\varepsilon}_{\alpha 1} - L\sqrt{3}\bar{\varepsilon}_{\alpha 2} \end{aligned}\right\}. \tag{35}$$

Now substitute (35) into (25)–(27) to obtain the reduced kinematic statement $\bar{\boldsymbol{B}} \cdot \bar{\boldsymbol{d}} = \bar{\boldsymbol{e}}$

$$\begin{pmatrix} -\frac{1}{2} & -\frac{\sqrt{3}}{2} & \frac{1}{2} & \frac{\sqrt{3}}{2} & 0 & 0 \\ 0 & 0 & -1 & 0 & 1 & 0 \\ \frac{1}{2} & -\frac{\sqrt{3}}{2} & 0 & 0 & -\frac{1}{2} & \frac{\sqrt{3}}{2} \\ \frac{1}{2} & \frac{\sqrt{3}}{2} & -\frac{1}{2} & -\frac{\sqrt{3}}{2} & 0 & 0 \\ 0 & 0 & 1 & 0 & -1 & 0 \\ -\frac{1}{2} & \frac{\sqrt{3}}{2} & 0 & 0 & \frac{1}{2} & -\frac{\sqrt{3}}{2} \end{pmatrix} \cdot \begin{Bmatrix} d_1^{(1)} \\ d_2^{(1)} \\ d_1^{(2)} \\ d_2^{(2)} \\ d_1^{(3)} \\ d_2^{(3)} \end{Bmatrix} = \begin{Bmatrix} e_1 \\ e_2 \\ e_3 - g_3(\bar{\boldsymbol{\varepsilon}}) \\ e_4 - g_4(\bar{\boldsymbol{\varepsilon}}) \\ e_5 - 2L\bar{\varepsilon}_{11} \\ e_6 + g_6(\bar{\boldsymbol{\varepsilon}}) \end{Bmatrix}, \tag{36}$$

where $g_3(\bar{\boldsymbol{\varepsilon}}) \equiv (\bar{\varepsilon}_{11} - \sqrt{3}\bar{\varepsilon}_{12})L$, $g_4(\bar{\boldsymbol{\varepsilon}}) \equiv (\bar{\varepsilon}_{11} + 3\bar{\varepsilon}_{22} + 2\sqrt{3}\bar{\varepsilon}_{12})L/2$ and $g_6(\bar{\boldsymbol{\varepsilon}}) \equiv (\bar{\varepsilon}_{11} - 3\bar{\varepsilon}_{22})L/2$. Straightforward row operations on (36) imply

$$\begin{pmatrix} -\frac{1}{2} & -\frac{\sqrt{3}}{2} & \frac{1}{2} & \frac{\sqrt{3}}{2} & 0 & 0 \\ 0 & 0 & -1 & 0 & 1 & 0 \\ \frac{1}{2} & -\frac{\sqrt{3}}{2} & 0 & 0 & -\frac{1}{2} & \frac{\sqrt{3}}{2} \end{pmatrix} \cdot \begin{Bmatrix} d_1^{(1)} \\ d_2^{(1)} \\ d_1^{(2)} \\ d_2^{(2)} \\ d_1^{(3)} \\ d_2^{(3)} \end{Bmatrix} = \begin{Bmatrix} e_1 \\ e_2 \\ e_3 - g_3(\bar{\boldsymbol{\varepsilon}}) \end{Bmatrix} \tag{37}$$

and

$$\left.\begin{aligned} e_1 + e_4 &= \left(\bar{\varepsilon}_{11} + 3\bar{\varepsilon}_{22} + 2\sqrt{3}\bar{\varepsilon}_{12}\right)L/2 \\ e_2 + e_5 &= 2L\bar{\varepsilon}_{11} \\ e_3 + e_6 &= \left(\bar{\varepsilon}_{11} + 3\bar{\varepsilon}_{22} - 2\sqrt{3}\bar{\varepsilon}_{12}\right)L/2 \end{aligned}\right\}. \tag{38}$$

To search for possible strain-producing collapse mechanisms for a truss made from inextensible bars, we substitute $\boldsymbol{e} = \boldsymbol{0}$ into (38). The solution is $\bar{\boldsymbol{\varepsilon}} = \boldsymbol{0}$, and it is concluded that the Kagome lattice has *no* inextensional collapse mechanisms capable of producing macroscopic strain. A collapse mechanism does exist however with the property $\bar{\boldsymbol{\varepsilon}} = \boldsymbol{0}$. This mechanism is unit cell periodic and coincides with the Bloch-wave solution at $w_1 = w_2 = 0$, as shown in Fig. 7a.

5.4.2. *Cauchy–Born reduction of the equilibrium matrix*

We now search for states of self-stress which are unit-cell periodic and which do support macroscopic stress $\bar{\boldsymbol{\sigma}}$. Anti-periodic traction conditions on the Kagome lattice unit cell of Fig. 3b imply

$$\boldsymbol{f}^{(1)} + \boldsymbol{f}^{(4)} = \boldsymbol{f}^{(2)} + \boldsymbol{f}^{(5)} = \boldsymbol{f}^{(3)} + \boldsymbol{f}^{(6)} = \boldsymbol{0}. \tag{39}$$

Recall that $f_\alpha^{(l)} = f_\alpha(\boldsymbol{j}_l)$ for $l \in \{1,2,3\}$, $f_\alpha^{(4)} = f_\alpha(\boldsymbol{j}_1 + \boldsymbol{a}_1 - \boldsymbol{a}_2)$, $f_\alpha^{(5)} = f_\alpha(\boldsymbol{j}_2 - \boldsymbol{a}_2)$, and $f_\alpha^{(6)} = f_\alpha(\boldsymbol{j}_3 - \boldsymbol{a}_1)$. Application of (39) to the equilibrium statement $\boldsymbol{A} \cdot \boldsymbol{t} = \boldsymbol{f}$ yields the

reduced equilibrium relation $\bar{\boldsymbol{A}} \cdot \bar{\boldsymbol{t}} = \boldsymbol{0}$ given by

$$\begin{pmatrix} -\frac{1}{2} & 0 & \frac{1}{2} & \frac{1}{2} & 0 & -\frac{1}{2} \\ -\frac{\sqrt{3}}{2} & 0 & -\frac{\sqrt{3}}{2} & \frac{\sqrt{3}}{2} & 0 & \frac{\sqrt{3}}{2} \\ \frac{1}{2} & -1 & 0 & -\frac{1}{2} & 1 & 0 \\ \frac{\sqrt{3}}{2} & 0 & 0 & -\frac{\sqrt{3}}{2} & 0 & 0 \\ 0 & 1 & -\frac{1}{2} & 0 & -1 & \frac{1}{2} \\ 0 & 0 & \frac{\sqrt{3}}{2} & 0 & 0 & -\frac{\sqrt{3}}{2} \end{pmatrix} \cdot \begin{Bmatrix} t_1 \\ t_2 \\ t_3 \\ t_4 \\ t_5 \\ t_6 \end{Bmatrix} = \begin{Bmatrix} 0 \\ 0 \\ 0 \\ 0 \\ 0 \\ 0 \end{Bmatrix} \tag{40}$$

for the six bars as labelled in Fig. 4c. The relation (40) implies that there are three independent bar tensions: $t_1 = t_4$, $t_2 = t_5$, and $t_3 = t_6$. These three bar tensions support an arbitrary state of macroscopic stress $\{\bar{\sigma}_{11}, \bar{\sigma}_{22}, \bar{\sigma}_{12}\}$. They correspond to the three states of self-stress in the Bloch-wave formulation at $w_1 = w_2 = 0$, and are plotted in Fig. 9a–c.

A comparison of (40) and (36) reveals that $\bar{\boldsymbol{B}} = \bar{\boldsymbol{A}}^{\mathrm{T}}$, as one would expect from application of the principle of virtual work. This means that $\mathrm{Nul}(\bar{\boldsymbol{A}}) = \mathrm{Nul}(\bar{\boldsymbol{B}}^{\mathrm{T}})$, and the states of self-stress satisfying (40) may be interpreted kinematically as the bar elongations disallowed by a unit-cell periodic joint displacement field.

5.5. Macroscopic stiffness

In order to determine the macroscopic stiffness of the Kagome lattice, we assume that the tension t_k in each bar k is related to the bar elongation e_k by $t_k = EAe_k/L$, where E is the elastic modulus of the constituent truss material, A is the cross-sectional area of the truss members, and L is the member length. The strain energy per unit area of the unit cell of Fig. 3b is $W = t_k e_k/2S$, where the unit-cell area is $S = 2\sqrt{3}L^2$ and k sums from 1 to 6. The macroscopic stress–strain constitutive law is given by $\bar{\boldsymbol{\sigma}} = \partial W/\partial \bar{\boldsymbol{\varepsilon}} = \bar{\mathscr{L}} : \bar{\boldsymbol{\varepsilon}}$, where the components of the macroscopic stiffness tensor $\bar{\mathscr{L}}$ are given by

$$\bar{\mathscr{L}}_{\alpha\beta\gamma\delta} = \frac{\partial^2 W(\bar{\boldsymbol{\varepsilon}})}{\partial \bar{\varepsilon}_{\alpha\beta} \partial \bar{\varepsilon}_{\gamma\delta}} = \frac{EA}{LS} \frac{\partial e_k(\bar{\boldsymbol{\varepsilon}})}{\partial \bar{\varepsilon}_{\alpha\beta}} \frac{\partial e_k(\bar{\boldsymbol{\varepsilon}})}{\partial \bar{\varepsilon}_{\gamma\delta}} \quad \forall \alpha, \beta, \gamma, \delta \in \{1, 2\} \tag{41}$$

summed over $k \in \{1, 2, \ldots, 6\}$. Appendix A presents a summary of the conditions for uniqueness of the solution to the macroscopic boundary value problem according to the nature of $\bar{\mathscr{L}}$.

Recall that the anti-periodic tractions imply $t_1 = t_4$, $t_2 = t_5$ and $t_3 = t_6$. For consistency, we set $e_1 = e_4$, $e_2 = e_5$ and $e_3 = e_6$. The relation (38) becomes

$$\left.\begin{aligned} e_1 = e_4 &= \left(\bar{\varepsilon}_{11} + 3\bar{\varepsilon}_{22} + 2\sqrt{3}\bar{\varepsilon}_{12}\right) L/4 \\ e_2 = e_5 &= L\bar{\varepsilon}_{11} \\ e_3 = e_6 &= \left(\bar{\varepsilon}_{11} + 3\bar{\varepsilon}_{22} - 2\sqrt{3}\bar{\varepsilon}_{12}\right) L/4 \end{aligned}\right\}. \tag{42}$$

These relations give a unique prescription for the bar elongations for an arbitrary state of macroscopic strain. Substitution of (42) into (41) yields eight non-zero macroscopic

stiffness components:

$$3\bar{\mathscr{L}}_{1111} = 3\bar{\mathscr{L}}_{2222} = \bar{\mathscr{L}}_{1122} = \bar{\mathscr{L}}_{2211} = \bar{\mathscr{L}}_{1212} = \bar{\mathscr{L}}_{2121} = \bar{\mathscr{L}}_{1221} = \bar{\mathscr{L}}_{2112} = EA\sqrt{3}/8L. \tag{43}$$

Note that the isotropic tensor $\bar{\mathscr{L}}$ is positive-definite. Consequently, the Kagome lattice is macroscopically *stiff* for all macroscopic stress and strain states.

The matrix form of $\bar{\boldsymbol{\sigma}} = \bar{\mathscr{L}} : \bar{\boldsymbol{\varepsilon}}$ reads

$$\begin{Bmatrix} \bar{\sigma}_{11} \\ \bar{\sigma}_{22} \\ \bar{\sigma}_{12} \end{Bmatrix} = \frac{\bar{\rho}E}{8} \begin{pmatrix} 3 & 1 & 0 \\ 1 & 3 & 0 \\ 0 & 0 & 2 \end{pmatrix} \cdot \begin{Bmatrix} \bar{\varepsilon}_{11} \\ \bar{\varepsilon}_{22} \\ \bar{\varepsilon}_{12} \end{Bmatrix}, \tag{44}$$

where $\bar{\rho} = A\sqrt{3}/L$ is the first-order relative density of the Kagome lattice. The response is isotropic with an effective Young's modulus $\bar{E} = \bar{\rho}E/3$ and Poisson's ratio $\bar{\nu} = \frac{1}{3}$.

6. The triangular–triangular lattice

A close link exists between the Kagome lattice and the so-called triangular–triangular T–T lattice shown in Fig. 10. The T–T lattice has the same topology as the Kagome lattice and its in-plane elastic response is isotropic due to its three-fold symmetry. In fact, a finite collapse mechanism with a single degree of freedom causes the T–T lattice to expand volumetrically to the Kagome lattice. This is evident in a plot of unit cell area S versus the characteristic angle ω, see Fig. 11. The Kagome lattice is *extremal* in unit cell area S, and can be collapsed hydrostatically either by decreasing or increasing ω away from $\pi/3$. Full collapse of the angle ω to either zero or $2\pi/3$ causes the structure to take on the fully triangulated form; but this limit is not achievable due to interference of the bars and to the required jump in connectivity from 4 to 6.

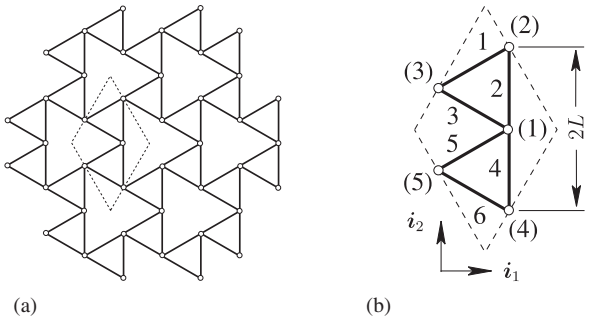

Fig. 10. (a) Triangular–triangular lattice with bar length L; (b) selected primitive unit cell with labelling required only for joints 1, 2 and 3.

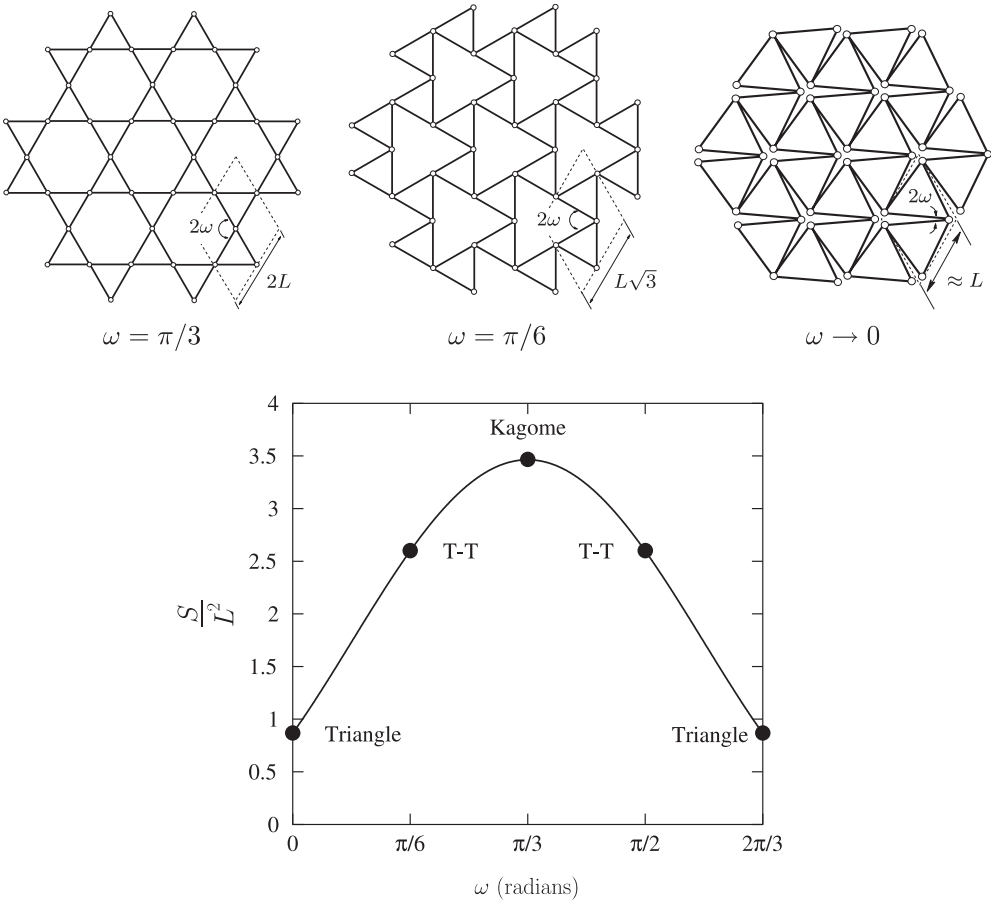

Fig. 11. Dependence of unit-cell area S upon angle ω. The Kagome lattice has $\omega = \pi/3$, the triangular–triangular lattice ("T–T") has $\omega = \pi/6$, and the triangular lattice has $\omega = 0$. All lattices have bar length L.

We proceed to consider the structural mechanics of the pin-jointed T–T truss. Preliminary analysis reveals that no infinitesimal periodic collapse modes exist. However, inextensional collapse modes do arise which produce macroscopic strain. These modes are analysed in the following section.

6.1. Mechanisms which generate macroscopic strain

6.1.1. Cauchy–Born reduction of the kinematic matrix

Consider the representative unit cell shown in Fig. 10b for the T–T lattice. It has the same topology as the Kagome unit cell of Fig. 3c, but has reduced symmetry. Infinitesimal collapse modes which generate macroscopic strain are postulated in accordance with the Cauchy–Born statement (19). The kinematic relation $\boldsymbol{B} \cdot \boldsymbol{d} = \boldsymbol{e}$ for the T–T lattice of Fig. 10b follows from the prescription (6). Using the orthonormal basis $\{\boldsymbol{i}_1, \boldsymbol{i}_2\}$ as shown in

Fig. 10b, we have

$$\boldsymbol{B} = \begin{pmatrix} 0 & 0 & \frac{\sqrt{3}}{2} & \frac{1}{2} & -\frac{\sqrt{3}}{2} & -\frac{1}{2} & 0 & 0 & 0 & 0 \\ 0 & -1 & 0 & 1 & 0 & 0 & 0 & 0 & 0 & 0 \\ \frac{\sqrt{3}}{2} & -\frac{1}{2} & 0 & 0 & -\frac{\sqrt{3}}{2} & \frac{1}{2} & 0 & 0 & 0 & 0 \\ 0 & 1 & 0 & 0 & 0 & 0 & 0 & -1 & 0 & 0 \\ \frac{\sqrt{3}}{2} & \frac{1}{2} & 0 & 0 & 0 & 0 & 0 & 0 & -\frac{\sqrt{3}}{2} & -\frac{1}{2} \\ 0 & 0 & 0 & 0 & 0 & 0 & \frac{\sqrt{3}}{2} & -\frac{1}{2} & -\frac{\sqrt{3}}{2} & \frac{1}{2} \end{pmatrix}, \tag{45}$$

$$\boldsymbol{d}^{\mathrm{T}} = [d_1^{(1)}\ d_2^{(1)}\ d_1^{(2)}\ d_2^{(2)}\ d_1^{(3)}\ d_2^{(3)}\ d_1^{(4)}\ d_2^{(4)}\ d_1^{(5)}\ d_2^{(5)}], \tag{46}$$

and

$$\boldsymbol{e}^{\mathrm{T}} = [e_1\ e_2\ e_3\ e_4\ e_5\ e_6]. \tag{47}$$

Now follow a similar methodology to that outlined in Section 5.4; the displacements of the boundary nodes (2–5) are related to the macroscopic strain $\bar{\boldsymbol{\varepsilon}}$ by

$$d_\alpha^{(4)} - d_\alpha^{(3)} = \left(\frac{\sqrt{3}}{2}\bar{\varepsilon}_{\alpha 1} - \frac{3}{2}\bar{\varepsilon}_{\alpha 2}\right)L \quad \text{and} \quad d_\alpha^{(2)} - d_\alpha^{(5)} = \left(\frac{\sqrt{3}}{2}\bar{\varepsilon}_{\alpha 1} + \frac{3}{2}\bar{\varepsilon}_{\alpha 2}\right)L. \tag{48}$$

Once these displacements are known, the position of the inner joint follows immediately. Upon applying (48) to (45)–(47), the reduced kinematic statement $\bar{\boldsymbol{B}} \cdot \bar{\boldsymbol{d}} = \bar{\boldsymbol{e}}$ is

$$\begin{pmatrix} 0 & 0 & \frac{\sqrt{3}}{2} & \frac{1}{2} & -\frac{\sqrt{3}}{2} & -\frac{1}{2} \\ 0 & -1 & 0 & 1 & 0 & 0 \\ \frac{\sqrt{3}}{2} & -\frac{1}{2} & 0 & 0 & -\frac{\sqrt{3}}{2} & \frac{1}{2} \\ 0 & 1 & 0 & 0 & 0 & -1 \\ \frac{\sqrt{3}}{2} & \frac{1}{2} & -\frac{\sqrt{3}}{2} & -\frac{1}{2} & 0 & 0 \\ 0 & 0 & -\frac{\sqrt{3}}{2} & \frac{1}{2} & \frac{\sqrt{3}}{2} & -\frac{1}{2} \end{pmatrix} \cdot \begin{Bmatrix} d_1^{(1)} \\ d_2^{(1)} \\ d_1^{(2)} \\ d_2^{(2)} \\ d_1^{(3)} \\ d_2^{(3)} \end{Bmatrix} = \begin{Bmatrix} e_1 \\ e_2 \\ e_3 \\ e_4 + g_4(\bar{\boldsymbol{\varepsilon}}) \\ e_5 + g_5(\bar{\boldsymbol{\varepsilon}}) \\ e_6 + g_6(\bar{\boldsymbol{\varepsilon}}) \end{Bmatrix}, \tag{49}$$

where $g_4(\bar{\boldsymbol{\varepsilon}}) = (\sqrt{3}\bar{\varepsilon}_{12} - 3\bar{\varepsilon}_{22})L/2$, $g_5(\bar{\boldsymbol{\varepsilon}}) = -(3\bar{\varepsilon}_{11} + 3\bar{\varepsilon}_{22} + 4\sqrt{3}\bar{\varepsilon}_{12})L/4$ and $g_6(\bar{\boldsymbol{\varepsilon}}) = (\sqrt{3}\bar{\varepsilon}_{12} - 3\bar{\varepsilon}_{11})L/2$. First, the null space of $\bar{\boldsymbol{B}}$ is examined in order to search for inextensional mechanisms ($\boldsymbol{e} = \boldsymbol{0}$) which produce no macroscopic strain ($\bar{\boldsymbol{\varepsilon}} = \boldsymbol{0}$). It is found that no such mechanisms exist. Second, we search for inextensional mechanisms which produce macroscopic strain. Row operations on (49) imply that

$$\left.\begin{aligned} e_1 - e_3 - e_4 + e_5 &= 3\left(\bar{\varepsilon}_{11} - \bar{\varepsilon}_{22} + 2\sqrt{3}\bar{\varepsilon}_{12}\right)L/4 \\ e_1 - e_2 - e_4 + e_6 &= 3(\bar{\varepsilon}_{11} - \bar{\varepsilon}_{22})L/2 \end{aligned}\right\}. \tag{50}$$

Inextensional mechanisms ($\boldsymbol{e} = \boldsymbol{0}$) satisfying (50) occur only for the equibiaxial strain state $\bar{\varepsilon}_{11} = \bar{\varepsilon}_{22}$ with $\bar{\varepsilon}_{12} = 0$. These collapse modes produce self-similar, volumetric contraction or dilation of the unit cell. This contraction or dilation is sketched in Fig. 11 wherein the unit-cell area S is parameterised by the angle ω shown.

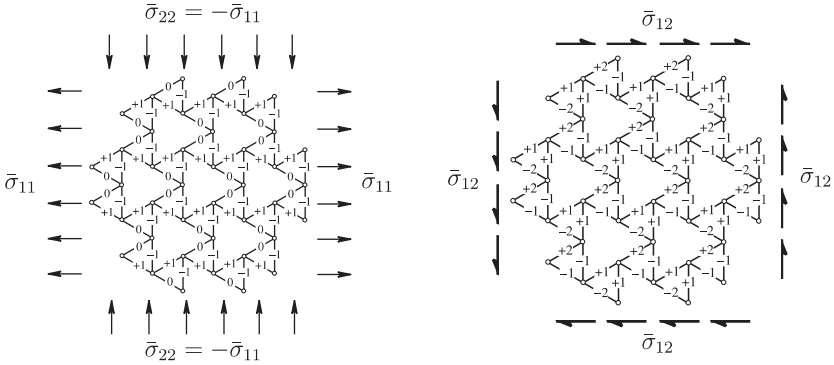

Fig. 12. States of self-stress in the triangular–triangular lattice for $w_1 = w_2 = 0$.

6.1.2. Cauchy–Born reduction of the equilibrium matrix

Recall that the Kagome lattice can support arbitrary macroscopic stress due to the fact that it has three internal states of self-stress. In contrast, the T–T lattice has a single strain-producing collapse mechanism ($\bar{\varepsilon}_{11} = \bar{\varepsilon}_{22}, \bar{\varepsilon}_{12} = 0$). Consequently, the T–T lattice is unable to support hydrostatic stress and has only two states of self-stress. We now search for these unit-cell periodic states of self-stress in the T–T lattice. Application of the Cauchy–Born, anti-periodic traction condition to the unit cell of Fig. 10b yields

$$\boldsymbol{f}^{(2)} + \boldsymbol{f}^{(5)} = \boldsymbol{0} \quad \text{and} \quad \boldsymbol{f}^{(3)} + \boldsymbol{f}^{(4)} = \boldsymbol{0}.$$

The unit cell equilibrium equation $\boldsymbol{A} \cdot \boldsymbol{t} = \boldsymbol{f}$ is thereby reduced to the form $\bar{\boldsymbol{A}} \cdot \bar{\boldsymbol{t}} = \boldsymbol{0}$ where $\bar{\boldsymbol{A}} = \bar{\boldsymbol{B}}^{\mathrm{T}}$, and $\bar{\boldsymbol{B}}$ has already been given in (49). Admissible bar tensions $\boldsymbol{t}$ in the reduced vector $\bar{\boldsymbol{t}}$ are those spanned by $\mathrm{Nul}(\bar{\boldsymbol{A}})$. These states of self-stress are sketched in Fig. 12, and they satisfy

$$\text{state 1:} \quad t_1 = -t_2 = -t_4 = t_6, \;\; t_3 = t_5 = 0 \tag{51}$$

and

$$\text{state 2:} \quad t_1 = t_2 = -\tfrac{1}{2}t_3 = -t_4 = \tfrac{1}{2}t_5 = -t_6. \tag{52}$$

The method of sections can be used to relate these bar tensions to the states of macroscopic stress. In state 1, we have $\{\bar{\sigma}_{11} = -\bar{\sigma}_{22}; \bar{\sigma}_{12} = 0\}$ while in state 2 we have $\{\bar{\sigma}_{11} = \bar{\sigma}_{22} = 0; \bar{\sigma}_{12} \neq 0\}$. Both states of self-stress are purely deviatoric. This is consistent with the hydrostatic collapse mechanism $\{\bar{\varepsilon}_{11} = \bar{\varepsilon}_{22}; \bar{\varepsilon}_{12} = 0\}$.

6.2. Macroscopic stiffness

The macroscopic stiffness tensor $\bar{\mathscr{L}}$ of the T–T lattice can be deduced from the strain energy density per unit area W of the unit cell. Assume that each bar tension t_k is related to the bar elongation e_k according to $t_k = EAe_k/L$, where A and L are the cross-sectional area and length of each bar, respectively and E is the Young' s modulus, as before. The strain energy density is $W = t_k e_k/2S$ where the unit cell area is $S = 3\sqrt{3}L^2/2$. The

macroscopic stress–strain constitutive law is again given by $\bar{\boldsymbol{\sigma}} = \partial W/\partial \bar{\boldsymbol{\varepsilon}} = \bar{\mathscr{L}} : \bar{\boldsymbol{\varepsilon}}$ and the components of the macroscopic stiffness tensor $\bar{\mathscr{L}}$ are given by (41).

Following the procedure of Section 5.5, we assume that the bar elongations in (50) are consistent with the states of self-stress (51) and (52) to obtain

$$\left.\begin{aligned} e_1 &= \left(3\bar{\varepsilon}_{11} - 3\bar{\varepsilon}_{22} + 2\sqrt{3}\bar{\varepsilon}_{12}\right)L/8 \\ e_2 &= \left(3\bar{\varepsilon}_{22} - 3\bar{\varepsilon}_{11} + 2\sqrt{3}\bar{\varepsilon}_{12}\right)L/8 \\ e_4 &= \left(3\bar{\varepsilon}_{22} - 3\bar{\varepsilon}_{11} - 2\sqrt{3}\bar{\varepsilon}_{12}\right)L/8 \\ e_6 &= \left(3\bar{\varepsilon}_{11} - 3\bar{\varepsilon}_{22} - 2\sqrt{3}\bar{\varepsilon}_{12}\right)L/8 \\ e_5 &= -e_3 = \bar{\varepsilon}_{12}L\sqrt{3}/2 \end{aligned}\right\}. \tag{53}$$

Then, using (53) in (41), the eight non-zero macroscopic stiffness components are:

$$\begin{aligned} \bar{\mathscr{L}}_{1111} &= \bar{\mathscr{L}}_{2222} = -\bar{\mathscr{L}}_{1122} = -\bar{\mathscr{L}}_{2211} = \bar{\mathscr{L}}_{1212} = \bar{\mathscr{L}}_{2121} = \bar{\mathscr{L}}_{1221} = \bar{\mathscr{L}}_{2112} \\ &= EA\sqrt{3}/8L. \end{aligned} \tag{54}$$

Note that $\bar{\mathscr{L}}$ is fourth-order symmetric, strongly elliptic and isotropic. The important point here is that the macroscopic stiffness tensor (54) violates pointwise stability but not strong ellipticity. Thus, the macroscopic prescribed-displacement boundary-value problem (BVP) has a unique solution whereas the prescribed-traction (or mixed) BVP does not (Triantafyllidis and Bardenhagen, 1996; Triantafyllidis and Schnaidt, 1993). Additional details are given in Appendix A.

In matrix form, the stiffness relation reads

$$\begin{Bmatrix} \bar{\sigma}_{11} \\ \bar{\sigma}_{22} \\ \bar{\sigma}_{12} \end{Bmatrix} = \frac{3\bar{\rho}E}{32} \begin{pmatrix} 1 & -1 & 0 \\ -1 & 1 & 0 \\ 0 & 0 & 2 \end{pmatrix} \cdot \begin{Bmatrix} \bar{\varepsilon}_{11} \\ \bar{\varepsilon}_{22} \\ \bar{\varepsilon}_{12} \end{Bmatrix}, \tag{55}$$

where $\bar{\rho} = 4\sqrt{3}A/3L$ is the first-order relative density of the T–T lattice. The non-uniqueness of the prescribed-traction BVP is consistent with the singular nature of (55). Specifically, $\bar{\boldsymbol{\sigma}}$ vanishes for all hydrostatic strain states, $\bar{\varepsilon}_{11} = \bar{\varepsilon}_{22}$ and $\bar{\varepsilon}_{12} = 0$, as demanded by the hydrostatic collapse mechanism shown in Fig. 11.

7. Concluding remarks

In this study matrix methods of linear algebra are combined with Bloch's theorem in order to determine the structural mechanics of the periodic, pin-jointed truss. Periodic collapse mechanisms and periodic states of self-stress are deduced from the four fundamental subspaces of the kinematic and equilibrium matrix for the periodic structure. The methodology developed is then applied to the Kagome lattice and the triangular–triangular T–T lattice. The Kagome lattice does not have macroscopic strain-producing mechanisms, but does passess periodic, inextensional collapse mechanisms.

The macroscopic elastic stiffness of a set of 2D, pin-jointed periodic lattices has been evaluated via the Cauchy–Born, uniform strain, hypothesis. It is shown that the Kagome lattice has macroscopic stiffness for all macroscopic loading states, and also possesses three unit-cell periodic states of self-stress in equilibrium with an arbitrary macroscopic stress state.

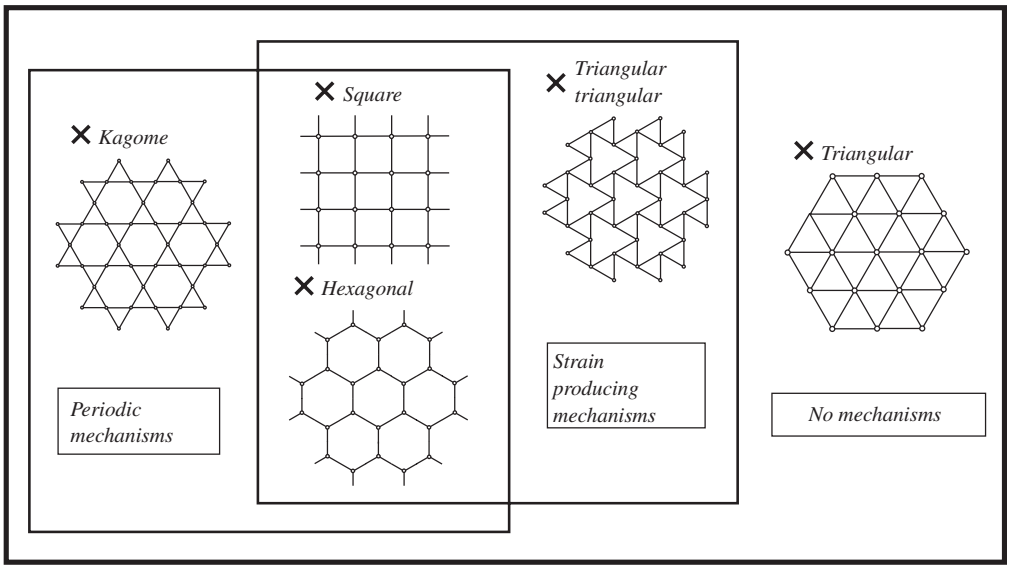

Fig. 13. Venn diagram summarising pin-jointed kinematics of selected planar trusses.

The T–T lattice is stiff except for the case of equibiaxial straining: it possesses a collapse mechanism of pure dilatation. Consequently, it can carry two arbitrary states of deviatoric macroscopic stress. Bloch wave analysis reveals that the T–T lattice has no periodic collapse mechanisms.

It is instructive to classify the structural performance of pin-jointed lattices. The square lattice has been re-visited recently by Hutchinson (2004) and the mechanics of the hexagonal lattice by Gibson and Ashby (1997). The square, hexagonal and Kagome lattices have periodic collapse mechanisms, while the square, hexagonal and T–T lattices have macroscopic strain-producing collapse mechanisms. The fully triangulated lattice has *neither* type of mechanism. Fig. 13 summarises these results in Venn diagram form.

The overall behaviours are consistent with the fact that periodic structures of low nodal connectivity ($Z = 3$ for the hexagonal lattice) contain strain-producing collapse mechanisms while periodic lattices of high nodal connectivity ($Z = 6$ for the triangulated lattice) are stiff under all macroscopic loading states. Periodic lattices with a connectivity of $Z = 4$ appear to be the transition case: the square lattice is stiff under some stress states, yet possesses macroscopic strain-producing collapse mechanisms. The Kagome lattice is stiff under all loading states, but it can collapse by periodic mechanisms which produce no macroscopic strain.

It is appreciated that practical lattice structures have joints which are neither pin-jointed nor rigid-jointed. The assumption of pin-joints is a useful approximation, however, for structures containing slender members, as the bending stiffness of the bars is much less than the axial stiffness.

The macroscopic stiffness of both 2D and 3D lattice materials is closely related to nodal connectivity. For example, open-celled foams with a nodal connectivity of 3–4 bars per joint rely upon the bending stiffness of joints and bars for macroscopic stiffness. In

pin-jointed configurations they would exhibit strain-producing collapse mechanisms. The octet truss on the other hand has a nodal connectivity of 12 and is stretching-dominated.

Acknowledgements

The authors are grateful for funding from a DARPA contract on synthetic multifunctional materials, and wish to thank A.G. Evans, J.W. Hutchinson, M.F. Ashby and V.S. Deshpande for helpful discussions.

Appendix A. Macroscopic strain energy density and uniqueness of macroscopic solution

Consider a unit cell $\mathbb{Y}$ of a periodic 2D pin-jointed truss made from linear elastic bars of length L. The unit cell is of area S and comprises b bars. We postulate the existence of a *macroscopic* (or *effective*) *strain energy density* defined, for the unit cell of b bars, as

$$W(\bar{\boldsymbol{\varepsilon}}) = \frac{1}{2}\bar{\boldsymbol{\sigma}}(\bar{\boldsymbol{\varepsilon}}) : \bar{\boldsymbol{\varepsilon}} = \frac{1}{2S} t_k(\bar{\boldsymbol{\varepsilon}}) e_k(\bar{\boldsymbol{\varepsilon}}). \tag{A.1}$$

Here, we sum over the repeated index k for $k \in \{1, \ldots, b\}$. The bar tensions are $t_k = (EA/L)e_k$ where, for each constituent (uniform) lattice member, E is the elastic modulus, A is the cross-sectional area, and L is the bar length. Kinematic and constitutive linearity assumed implies that $W(\bar{\boldsymbol{\varepsilon}})$ is a *quadratic form* in $\bar{\boldsymbol{\varepsilon}}$, and

$$\bar{\boldsymbol{\sigma}}(\bar{\boldsymbol{\varepsilon}}) = \frac{\partial W(\bar{\boldsymbol{\varepsilon}})}{\partial \bar{\boldsymbol{\varepsilon}}} = \bar{\mathscr{L}} : \bar{\boldsymbol{\varepsilon}} = \frac{EA}{LS} e_k(\bar{\boldsymbol{\varepsilon}}) \frac{\partial e_k(\bar{\boldsymbol{\varepsilon}})}{\partial \bar{\boldsymbol{\varepsilon}}}. \tag{A.2}$$

$\bar{\mathscr{L}}$ is the fourth-order, linearly elastic, *macroscopic stiffness tensor*, and its components may be calculated via

$$\bar{\mathscr{L}}_{\alpha\beta\gamma\delta} = \frac{\partial^2 W(\bar{\boldsymbol{\varepsilon}})}{\partial \bar{\varepsilon}_{\alpha\beta} \partial \bar{\varepsilon}_{\gamma\delta}} = \frac{EA}{LS} \frac{\partial e_k(\bar{\boldsymbol{\varepsilon}})}{\partial \bar{\varepsilon}_{\alpha\beta}} \frac{\partial e_k(\bar{\boldsymbol{\varepsilon}})}{\partial \bar{\varepsilon}_{\gamma\delta}} \quad \forall \alpha, \beta, \gamma, \delta \in \{1, 2\}, \tag{A.3}$$

where each component of $\partial e_k / \partial \bar{\varepsilon}_{\alpha\beta}$ is a *constant* and $\bar{\mathscr{L}}$ has the symmetries

$$\bar{\mathscr{L}}_{\alpha\beta\gamma\delta} = \bar{\mathscr{L}}_{\gamma\delta\alpha\beta} = \bar{\mathscr{L}}_{\alpha\beta\delta\gamma} = \bar{\mathscr{L}}_{\beta\alpha\gamma\delta}. \tag{A.4}$$

The following discussion regarding stability and uniqueness is based upon Gurtin (1972, 1981), Marsden and Hughes (1994), Ogden (1997), Simo and Hughes (1998) and Han and Reddy (1999). The macroscopic strain energy density function $W(\bar{\boldsymbol{\varepsilon}})$ is *convex*, and the macroscopic stiffness tensor $\bar{\mathscr{L}}$ is *pointwise stable* and *positive-definite*, if there exists a positive real β such that

$$\boldsymbol{\xi} : \bar{\mathscr{L}} : \boldsymbol{\xi} \geqslant \beta \, \boldsymbol{\xi} : \boldsymbol{\xi} \tag{A.5}$$

for all symmetric second-order tensors $\boldsymbol{\xi}$. When $\bar{\mathscr{L}}$ is positive-definite, uniqueness is ensured for *all* macroscopic boundary conditions.

Note that the macroscopic stiffness tensor $\bar{\mathscr{L}}$ satisfies the *strong ellipticity condition* if there exists a positive real α such that

$$\boldsymbol{a} \otimes \boldsymbol{b} : \bar{\mathscr{L}} : \boldsymbol{a} \otimes \boldsymbol{b} \geqslant \alpha \|\boldsymbol{a}\|^2 \|\boldsymbol{b}\|^2 \quad \forall \boldsymbol{a}, \boldsymbol{b} \in \mathbb{R}^2. \tag{A.6}$$

This is true when the macroscopic acoustic tensor $\bar{\mathscr{L}}_{\alpha\beta\gamma\delta} b_\beta b_\delta$ is positive-definite. Physically, this implies that all possible macroscopic wave speeds are real (not imaginary) and ensures the elliptic character of the governing macroscopic equilibrium equations. Inequality (A.6)

ensures *uniqueness* for the macroscopic, *prescribed-displacement* problem and precludes highly localised solutions (e.g. shear bands). Note that pointwise stability implies strong ellipticity but *not* conversely.

References

Ashby, M.F., Evans, A.G., Fleck, N.A., Gibson, L.J., Hutchinson, J.W., Wadley, H.N.G., 2000. Metal Foams: A Design Guide. Butterworth-Heinemann, Boston.

Bhattacharya, K., 2003. Microstructure of martensite: why it forms and how it gives rise to the shape-memory effect. Oxford Series on Materials Modelling, vol. 2. Oxford University Press, New York.

Bloch, F., 1928. Über die Quantenmechanik der Elektronen in Kristallgittern. Z. Physik 52, 555–599.

Born, M., Huang, K., 1954. Dynamical Theory of Crystal Lattices. Clarendon Press, Oxford.

Brillouin, L., 1946. Wave propagation in periodic structures: electric filters and crystal lattices. International Series in Pure and Applied Physics. McGraw-Hill, New York.

Cantrell, C.D., 2000. Modern Mathematical Methods for Physicists and Engineers, first ed., Cambridge University Press, Cambridge.

Christensen, R.M., 2000. Mechanics of cellular and other low-density materials. Int. J. Solids Struct. 37, 93–104.

Coates, R.C., Coutie, M.G., Kong, F.K., 1998. Structural Analysis, third ed., Chapman & Hall, London.

Cornwell, J.F., 1997. Group Theory in Physics: An Introduction. Academic Press, San Diego.

Crandall, S.H., Dahl, N.C., Lardner, T.J., 1978. An Introduction to the Mechanics of Solids, second ed., McGraw-Hill, New York.

Deshpande, V.S., Ashby, M.F., Fleck, N.A., 2001a. Foam topology: bending versus stretching dominated architectures. Acta Materialia 49 (6), 1035–1040.

Deshpande, V.S., Fleck, N.A., Ashby, M.F., 2001b. Effective properties of the octet-truss lattice material. J. Mech. Phys. Solids 49, 1724–1769.

Gibson, L.J., Ashby, M.F., 1997. Cellular Solids: Structure and Properties, second ed. Cambridge Solid State Science Series. Cambridge University Press, Cambridge (First paperback (1999) edition with corrections).

Grosso, G., Pastori-Parravincini, G., 2000. Solid State Physics. Academic Press, London.

Guest, S.D., Hutchinson, J.W., 2003. On the determinacy of repetitive structures. J. Mech. Phys. Solids 51, 383–391.

Gurtin, M.E., 1972. The linear theory of elasticity. In: Truesdell, C. (Ed.), Handbuch der Physik, vol. VIa/2: Mechanics of Solids II. Springer, Berlin, pp. 1–295.

Gurtin, M.E., 1981. An introduction to continuum mechanics. Mathematics in Science and Engineering, vol. 158. Academic Press, New York.

Han, W., Reddy, B.D., 1999. Plasticity: mathematical theory and numerical analysis. Interdisciplinary Applied Mathematics, vol. 9. Springer, New York.

Hilbert, D., Cohn-Vossen, S., 1990. Geometry and the Imagination. American Mathematical Society, Providence, RI (Republication of (1952) Chelsea edition, New York).

Hutchinson, R.G., October 2004. Mechanics of lattice materials. Ph.D. Dissertation, Department of Engineering, University of Cambridge.

Hutchinson, R.G., Fleck, N.A., 2005. Microarchitectured cellular solids—the hunt for statically determinate periodic trusses. ZAMM 85, 607–617.

Hyun, S., Torquato, S., 2002. Optimal and manufacturable two-dimensional kagome-like cellular solids. J. Mater. Res. 17 (1), 137–144.

Jones, W., March, N.H., 1973. Theoretical Solid State Physics: Perfect Lattices in Equilibrium, vol. 1. Wiley-Interscience, London.

Livesley, R.K., 1975. Matrix methods of structural analysis. Pergamon International Library of Science, Technology, Engineering and Social Studies, second ed., Pergamon Press, Oxford.

Lomont, J.S., 1959. Applications of Finite Groups. Academic Press, New York.

Marks, R.W., 1960. The Dymaxion World of Buckminster Fuller. Reinhold, New York.

Marsden, J.E., Hughes, T.J.R., 1994. Mathematical Foundations of Elasticity. Dover, New York Corrected Republication of (1983) Prentice-Hall edition, Englewood Cliffs.

Maugin, G.A., 1992. The thermomechanics of plasticity and fracture. Cambridge Texts in Applied Mathematics. Cambridge University Press, Cambridge.

Maxwell, J.C., 1864. On the calculation of the equilibrium and stiffness of frames. Philos. Mag. 27, 294–299 (Paper XXVI in Collected papers, Cambridge 1890).

Ogden, R.W., 1997. Non-linear Elastic Deformations. Dover, New York Corrected Republication of (1984) Ellis Horwood edition, New York.

Pellegrino, S., 1993. Structural computations with the singular value decomposition of the equilibrium matrix. Int. J. Solids Struct. 30 (21), 3025–3035.

Pellegrino, S., Calladine, C.R., 1986. Matrix analysis of statically and kinematically indeterminate frameworks. Int. J. Solids Struct. 22 (4), 409–428.

Pitteri, M., Zanzotto, G., 2003. Continuum Models for Phase Transitions and Twinning in Crystals. Chapman & Hall/CRC Press, Boca Raton.

Przemieniecki, J.S., 1968. Theory of Matrix Structural Analysis, second ed., McGraw-Hill, New York.

Simo, J.C., Hughes, T.J.R., 1998. Computational inelasticity. Interdisciplinary Applied Mathematics, vol. 7. Springer, New York.

Symons, D.D., Hutchinson, R.G., Fleck, N.A., 2005. Actuation of the Kagome double-layer grid. Part 1: prediction of performance of the perfect structure. J. Mech. Phys. Solids 53, 1855–1874.

Tantikom, K., Yoshihiro, S., Aizawa, T., 2004. In-plane compression response of regularly cell-structured materials. Mater. Trans. 45 (2), 509–515.

Torquato, S., Gibiansky, L.V., Silva, M.J., Gibson, L.J., 1998. Effective mechanical and transport properties of cellular solids. Int. J. Mech. Sci. 40, 71–82.

Triantafyllidis, N., Bardenhagen, S., 1996. The influence of scale size on the stability of periodic solids and the role of associated higher order gradient continuum models. J. Mech. Phys. Solids 44 (11), 1891–1928.

Triantafyllidis, N., Schnaidt, W.C., 1993. Comparison of microscopic and macroscopic instabilities in a class of two-dimensional periodic composites. J. Mech. Phys. Solids 41 (9), 1533–1565.

Triantafyllidis, N., Schraad, M.W., 1998. Onset of failure in aluminum honeycombs under general in-plane loading. J. Mech. Phys. Solids 46 (6), 1089–1124.